UNIVERSITÀ DEGLI STUDI DI PADOVA

UNIVERSITA' DEGLI STUDI DI PADOVA

Dipartimento di Ingegneria Industriale DII

Corso di Laurea Magistrale in Ingegneria Meccanica

Analisi fluidodinamica e ottimizzazione di schiere palari per compressori transonici

Relatore: Prof. Ernesto Benini

Correlatore: Ing. Giovanni Venturelli

Laureando: Francesco Maria Ferrari

Mat. 1061186

Anno Accademico 2014/2015

Abstract

The aim of this study is to understand the physical phenomena on basis of transonic compressor blade and to find the geometrical parameters that more influence the performance of the blade. This is achieved simulating a certain typologies of transonic compressor blades, starting from the very first that is Kantrowitz blade, through the Double Circular Arc blade and Multiple Circular Arc blade, till the last s-shape blade that represents the state of art. In this thesis has been considered planar blade cascade, so all the study is focused on two-dimensional geometry. This allows to concentrate the attention on shock wave system and on all the two-dimensional sources of loss. The blades listed above have been sketched with a solid modeler, hence meshed with ANSYS® ICEM by the use of a structural mesh, and finally simulated with the numerical solver ANSYS® Fluent v14. The results obtained from numerical simulations have been compared with the experimental ones in order to validate the them. All the blades appear to trace the experimental test also considering that experimental tests are not perfectly two-dimensional as numerical simulation (AVDR influence). Comparing the fluid domain of all the blades, it's clear that the most important region is the former zone of the suction side, because here the shock waves takes place and so modifying the shape of this zone is possible to have a more efficient blade. It has been highlighted that the concave curvature in the suction side produces a system of pre-compression waves and an oblique passage shock that is more efficient than the passage normal shock that appears in the other blades. Considering the importance of this zone, has been realized an optimization process of the s-shape blade, keeping fix all the coordinates of the blade except for this zone that has been parametrized by the use of Bèzier curve. The optimization has been conducted with the genetic algorithm implemented in Matlab giving the following options: 7 individuals and 3 generations. The optimization revealed a great potentiality of this former zone of the blade, in fact starting from a value of loss coefficient of 0.981 the optimization leads to a value of 0.0942 with an improvement in performance of 4.2%.

Contents

Nomenclature and conventions

Abbreviations

c_θ	tangential velocity component
U	peripheral velocity
β	flow angle of relative velocity
γ	stagger angle
M	Mach number
k	ideal gas constant
AVDR	axial velocity density ratio
DCA	Double circular arc
MCA	Multiple circular arc
DOF	decision variables
GA	genetic algorithm
LE	leading edge
TE	trailing edge
SS	suction side
PS	pressure side

Subscripts and superscripts

1 inlet
2 outlet
∞ upstream the blade

1 Introduction

Today most of aircraft engines use transonic compressors because they can operate with high pressure ratios and high efficiency, so it is possible to realize engines reducing weight and size; thereby reducing the operational costs.
The great advantages of using supersonic compressors had been discovered since the '40s of the past century starting from the study conducted on supersonic diffusers by Arthur Kantrowitz and Coleman duP.Donaldson[1] and later by Arthur Kantrowitz in "*The supersonic axial-flow compressor"*[2]. However, at that time, the reasons which limited the widespread of this kind of compressors was the presence of large energy losses at speeds higher than the speed of sound. Because of the supersonic inlet flow "shock wave phenomena arise in the inlet flow and passage region drastically affecting the efficiency of the machine"[3], there are two type of losses: the entropy rise due to the shock, and the interaction shock-boundary layer.
The complexity of the phenomena arising in this kind of blade and the limited computational instruments available in the past led to modify the shape of blades without a complete knowledge of the physic of the system. So many changes had been conducted only basing on the experimental tests realized on the blades trying lots of shape; and also today for the last s-shape compressor blades the physics bases which regulate the fluid dynamic behavior are not completely known. The aim of this thesis is to try to understand the physical phenomena on the basis of transonic compressor blades and then starting from this knowledge to choose the geometric parameters of the blades which most influence blade's behavior, Hence an optimization it has been realized of today's state of art compressor blades that are s-shape profiles.
This study is composed by a first part where the most important transonic compressor blades are described and simulated: starting from Kantrowitz's one to s-shape passing throw circular arc blade(CA) and multiple circular arc blade(MCA); these blades have been sketched with a solid modeler so they have been meshed with ICEM and simulated with ANSYS Fluent. The results of simulations have been compared with experimental results reported on specific papers. After validation, the results of these several blades have been compared and analyzed to understand how changing in geometry involves changing in performance and so it has been possible to choose the most important geometric parameters for optimization, using a genetic algorithm.
All this study has been developed on a linear cascade which means that all simulations has been conducted on a 2D section of the blade. Even if the real flow in a 3D-shapes compressor rotors is strongly three dimensional, a cascade study is a good starting point to understand how to reduce the losses related with shock waves. In this way this work is focused on the aerodynamic losses and

analyzing the cascade it is possible to concentrate only on this kind of losses isolating other sources of loss mechanism.

2 Transonic compressors

Transonic axial compressors are compressing machine operating with supersonic velocities relative to the blading.

This compressors provide higher pressure ratios than subsonic one ,so it is possible to reduce the number of stage of a compressor fan and so the total weight and size of the engine; this becomes useful particularly in aircraft applications. Advantages of using transonic compressors derive directly from Euler's momentum equation:

$h=(U_2*c_{\theta 2}-U_1*c_{\theta 1})$

This equation shows that two parameters regulates the enthalpy exchange: the absolute flow turning c_θ that however is restricted under certain limits, and the blade speed U which consequently implies the increase in relative inlet velocity. Transonic compressors are so composed by a first part near the outer span where relative velocities are supersonic and a second part towards the hub of the blade where relative velocities are subsonic.

Hence, ideally a transonic compressor blade could be divided in a first part that is dominated by system shock wave that starts from the leading edge and covers the blade passage, and a second part where the flow is subsonic and the compression of the fluid occurs throw the blade shape. The great challenge is to obtain compressors which can operate at higher pressure ratio but also with high efficiency, this because transonic compressors operate with a complex system of shock waves and this involve an increase in loss. In fact all shock waves are an irreversible event with consequently increasing in entropy of the system, moreover the interaction between shock wave and secondary flows (tip clearance) and the boundary layer has a negative impact on the flow field. Generally losses can be divided in two great groups: shock losses across the passage between two leading edge, and profile losses. This separation is only conceptual but not physical because shock waves generate boundary separation so the two kind of losses are related each other. The shock wave pattern is influenced by geometry of blade, inlet Mach number , inlet flow direction and back pressure at the outlet of the blade. Moreover the curvature radius at leading edge is minimized in order to reduce the risk of having a normal shock in the front part according to what is shown in Figure (2.1):

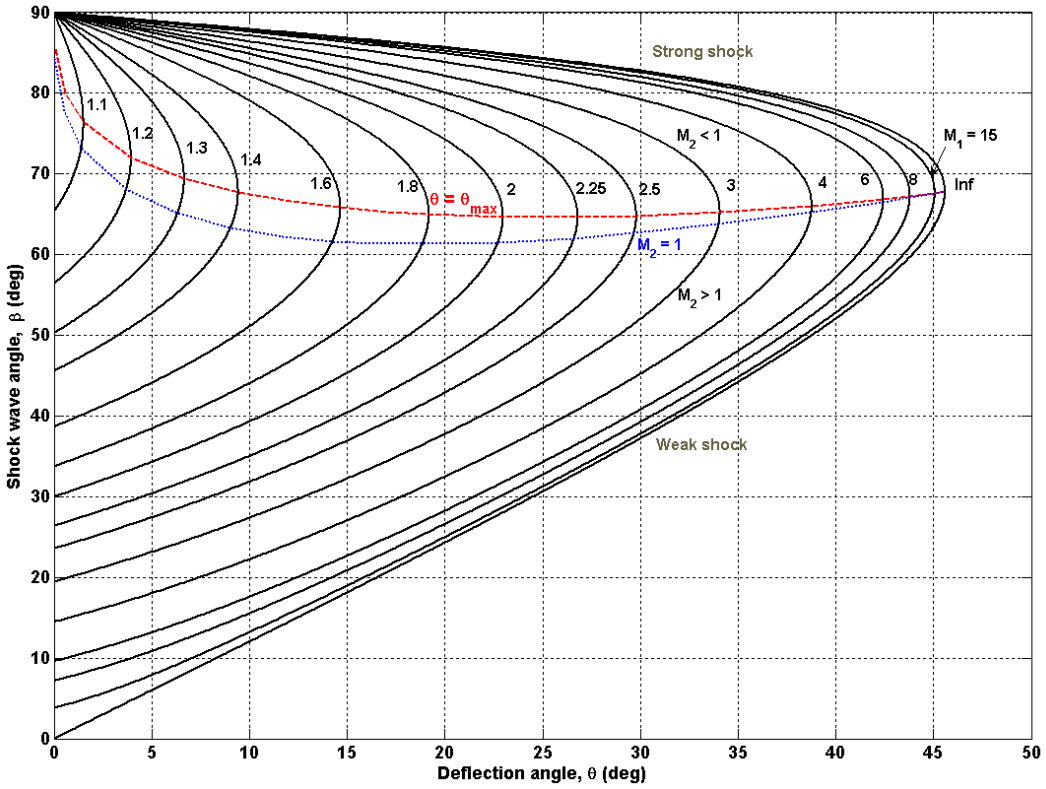

Figure 2.1 : Shock wave angle in function of deflection angle

So reducing the deflection angle (and so the blade thickness) also with great Mach numbers the bade experiences oblique shock that is more efficient than normal shock.

2.1Unique Incidence

Although velocity relative to the blade is supersonic, two possibilities are available for axial component that could be supersonic or subsonic:

1. M_{1x}>1 this means that the flow upstream the cascade is not influenced by the cascade itself; all the shock and expansion waves are enveloped by blade passage, this because the supersonic axial flow does not allow information to go back forward the cascade.
2. M_{1x}<1in this case the subsonic axial velocity allow the information to go back upstream and so shock and expansion waves can condition the incoming flow.

This study is focused on supersonic relative velocity at inlet, but with subsonic axial component and subsonic Mach number at outlet, that are more interesting conditions for transonic compressors. In these conditions “if the inlet Mach

number is sufficiently high, the cascade operates along the so called unique incidence curve"[3].

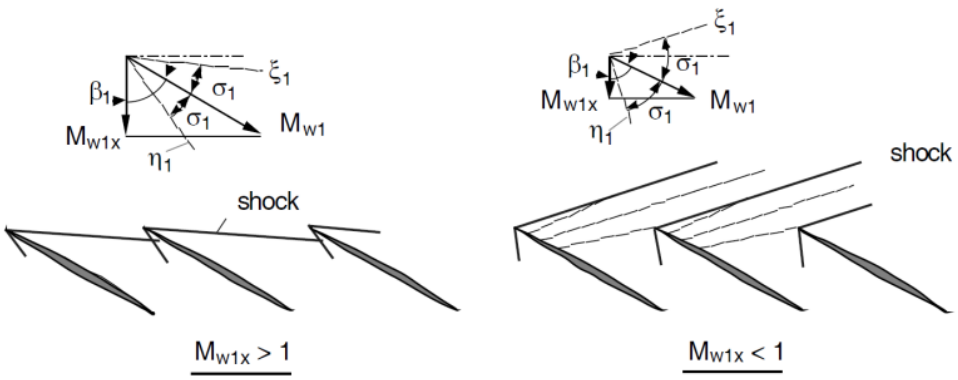

Figure 2.2: Supersonic flow in blade row

Unique incidence curve is a curve that join inlet Mach number and flow direction, that means, within a range of back pressure and for a given geometry of the blade and particularly of leading edge, is impossible modify Mach number without modifying the flow direction.

2.1.1Unique incidence behavior

To concretely explain the unique incidence phenomenon we can consider a flat plate cascade with a flow direction of β_∞ different from the stagger angle γ. Two cases are possible depending on negative or positive incidence of incoming flow over the first blade:

1. Positive incidence: in this case the incoming flow generates a series of Prandtl-Meyer expansion waves centered on the leading edge, this involves an acceleration of flow, up to $M_1$and the flow is deflected towards the plate direction till β_1=γ. In this way ,because of the subsonic axial velocity, the waves perturb the flow ahead and all the other blades except the first experience a flow of Mach number $M_1$and flow angle γ ,so approaches the blades with null incidence.
2. Negative incidence: in this case the opposite direction of incoming flow generates compression waves centered on the leading edge and in a symmetrical way than the upper case Mach number decrease to $M_1$and, always under the condition of subsonic axial velocity, the flow direction moves towards γ for the blades different from the first.

In both these situations is possible to distinguish two different situations in which the flow meets the blade; one represented by the first blade which is hit by a flow of relative velocity M_∞ and direction β_∞, as this flow sets the condition for the remaining blades. And a second situation represented by the other blades which experience an inlet flow of $M_1$and β_1.

Now is important notice that if the flow changes his direction from β_∞ to a new value of β_∞^1 the first blade adapts the waves system in a way that the other blades will experience however β_1=γ. This means that even if the incoming flow changes angle, the blades different from the first experience always the same direction.
From this observation immediately derives the conclusion that if the cascade is composed by an infinite number of plate blades, there is not a first blade and so all blades experience a Mach number $M_1$and a flow direction β_1. Hence there is a great difference between the semi-infinite and infinite cascade about the incoming flow: in the first case the blades could experience values of M_∞ and β_∞ different than $M_1$and β_1 depending if the flow approaches the first blade or the others. In the second case flow hits the blades with same value M_1 and β_1 ,because of the Mach lines that departs from suction surface and go in front of the cascade. In this particular case of flat plate the Prandtl-Meyer waves adapt the flow till β_1=γ, independently of the Mach number that approach the blades β_1=γ, $\forall$ M_1; this is evidently shown in Figure(2.3) where the inlet flow angle β_1 is plotted again the inlet Mach number $M_1$where in this particular case for a limited range of back pressure the unique incidence curve is a horizontal line.

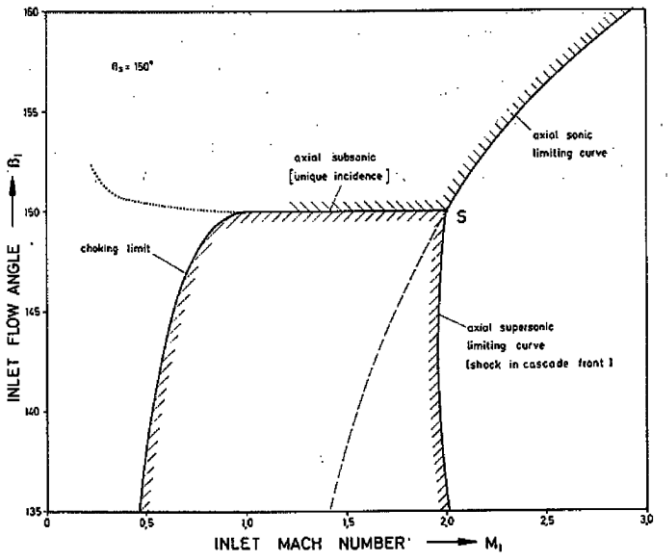

Figure 2.3: **Inlet flow angle for a flat plane cascade [4]**

In the case of S-shape profile even if the analysis is more complicated, the idea of unique incidence is the same. In this case the curve is not linear the relation is different from flat plate, but however there is a specific relation between the flow direction and the inlet Mach number:

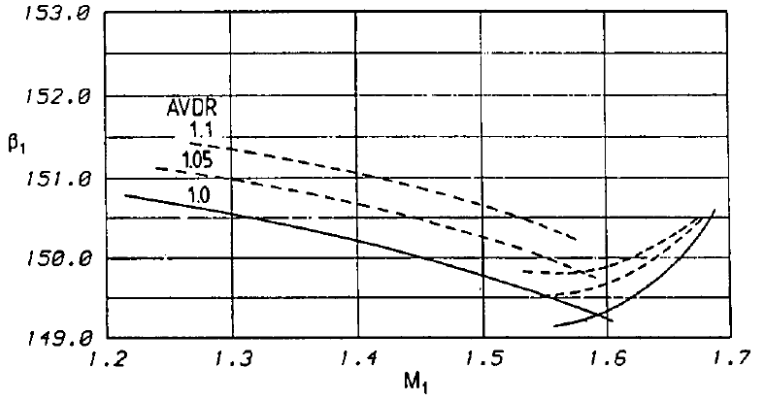

Figure 2.4: Inlet flow angle in function of inlet Mach number of S-shape cascade [5]

In conclusion this is a simple and easier explanation of unique incidence than more complex analysis on cambered profile. Reassuming in a certain range of static back pressure is not possible to change independently Mach number and flow direction, this phenomenon is the result of three conditions:

- Subsonic axial flow direction M_{1x}<1, therefore the presence of the cascade can affect the inlet flow through expansion and compression waves.
- Periodic condition, so the inlet flow characteristics must repeat for all the blades of the cascade.
- The attached shock wave behaves as a wall for the information coming from the outlet, preserving the inlet flow from any changing.

2.1.2 Started and unstarted condition

In the previous chapter it has been already said that unique incidence occurs only for a limited operating pressure range. Figure(2.5) shows what happens to waves increasing the static back pressure and inlet conditions are fixed.

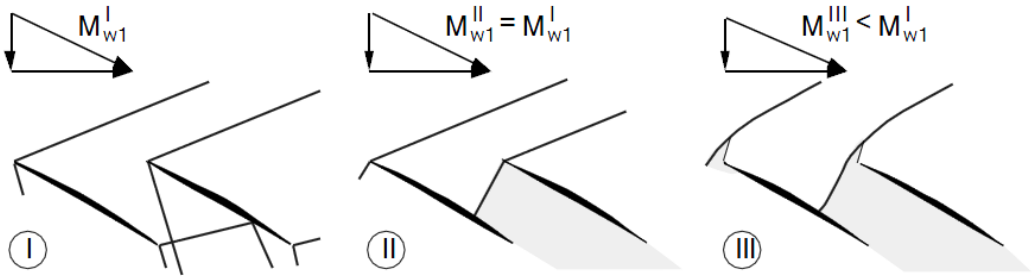

Figure 2.5: Supersonic flow in a compressor cascade at different pressures [6]

This picture shows left to right the movement of the shock wave increasing the back pressure. In the first two images the shock pattern is yet confined in the blade passage and attached to the leading edge, in this case an increase in back pressure force the wave to move to passage entrance. Shock wave in this condition behave like a wall for the information coming from outlet and an

increase of backpressure does not involve any change in the inlet flow, in this condition the cascade is started. The second image depicts a limit situation at this condition(shock exactly at passage entrance) called spill point; further increase in pressure generates a detached shock (picture III) leading to the unstarted condition, in which static back pressure influence inlet flow. Beside the spill point the unique incidence is not good any more and a new relation occurs between inlet Mach number and flow direction parametric with static back pressure. Condition two represent the higher static back pressure for working at unique incidence for a given inlet Mach number, there is also a limit to lower Mach number, under this limit attached wave is not possible and the cascade works in unstarted condition. Finally the unique incidence represent a chocked condition; in fact a back pressure changing does not involve a variation of inlet flow, hence mass flow remains unchanged. Spill point is also the condition of maximum efficiency of the cascade.

2.1.3Theoretical and experimental considerations

Under the hypothesis of irrotational and isentropic flow the system of Prandtl-Meyer waves obeys to the theory of Riemann invariant:

$\beta_\infty+\nu(M_\infty)= \beta_1+\nu(M_1)$

$\nu(M)=\left(\frac{k+1}{k-1}\right)^{0.5}\arctan\left[\frac{k-1}{k+1}(M^2-1)\right]^{0.5}$-$\arctan[M^2-1]^{0.5}$

Looking at this equation, any changing at Mach number or flow direction produces a consequently changing of the other parameter, for keeping the invariant constant.

"Another consequence of these hypothesis is the existence of *characteristics* curves along which the Mach number and flow angle are constant. As for supersonic cascades, characteristics have usually got a linear pattern"[3].

When the inlet flow coming from the nozzle (M_∞, β_∞) differs from unique incidence conditions, the system adapt the flow through expansion or compression waves, respectively if the inlet flow direction is lower or higher than β_1. These two systems have a different impact on the isentropic and irrotational conditions of Riemann invariant. The expansion waves modify the flow accelerating it in a quasi-isentropic way, on the other hand the compression one tend to decelerate the flow increasing entropy. So it is clear that expansion waves follow more rigorously the Riemann invariant conditions.

Many experimental proofs shown in the following chapters has been performed in a wind tunnel. A cascade tested in a wind tunnel can be assimilated to a semi-infinite cascade in which the first blade fixes the appropriate inlet flow conditions (M_1, β_1); experimental results show that this apparatus can be considered with good approximation two dimensional, isentropic and irrotational up to the incoming shock wave, so for the inlet region is justify the use of Riemann

invariant. “In fact, supersonic blades are usually characterized by thin leading edges and low front chamber, which minimize total pressure losses related with the inlet wave pattern”[3].

2.2 Unique incidence control loop

How is it possible to know the value of M_1 and β_1, characteristics of unique incidence? These values are not boundary conditions any more, but are results of interaction between the incoming flow and the cascade, in fact the subsonic axial flow allow the information to come upstream in axial direction and the shock wave to affect the inlet conditions. So to honor the periodicity the infinite flow (M_∞, β_∞) is deflected till (M_1, β_1) by a shock wave system always respecting the constancy of Riemann invariant, this is the reason why (M_1, β_1) cannot be considered as results of boundary conditions but as results of calculation.
Practically this condition is recreates in Fluent using as inlet boundary condition *pressure-far-field*, where M_∞ and β_∞ are fixed by user, so the software can estimates Riemann invariant β_∞+ν(M_∞). “The Riemann invariant is the joining link between the infinite and the inlet boundary”[3], hence Fluent is able to calculate the inlet conditions (M_1, β_1).
Now is clear that is impossible to calculate in an analytical way the inlet conditions, so it is necessary to realize a recursive procedure to find them. Before describing the iterative procedure realized, it is important to fix two variables which influence UI:

- M_1(orβ_1) : the constancy of Riemann invariant and fixing M_1(orβ_1) allow to completely describe the inlet conditions as following described.
- $p2$: the static back pressure should be sufficiently low to avoid the passing of spill point and so the loss of UI. In this way the flow domain is independent from back pressure and can research the value of (M_∞, β_∞) to reach the inlet Mach number M_1.

Fixed this two variables is now possible to found the inlet conditions (M_1, β_1).
The loop strategy is based on the consideration that according to what already said on UI it is possible to approximate unique incidence curve to a linear model. Hence this loop starts from (M_∞, β_∞), where M_∞ is fixed as M_{target} and is kept constant during the iterations as shown in Figure(2.6),whereas β_∞ is modified step by step to reach (M_{target}=M_∞, β_1).The iteration step are shown in Figure(2.6): 1) the starting point is (M_∞, β_∞), with β_∞ is arbitrarily selected;2) from this point the system comes to point (M_1, β_1) by means of a flow simulation realized with Fluent which preserve the Riemann invariant. 3) The new point for the second CFD simulation is founded by tracing a casual “A priori” UI curve with an arbitrary slope and intersecting it with the vertical of M_{target}, this point represent the starting point for the second simulation with coordinates (M_∞, β_∞), where

M_{target}=M_∞ so Mach number does not change, but flow direction assume a new value for β_∞. 4) The new point (M_1, β_1) is founded carrying out a second CFD simulation, this new point has a different Mach number from M_{target}, so is necessary to come back to M_{target}. 5) So from the second iteration and for all the remaining, the new point (M_{target}=M_∞, β_1) is founded tracing the line passing through the last two simulated points and intersecting it with the vertical line correspondent to M_{target}. 6) This procedure has been repeated until difference between the point simulated and M_{target} is sufficiently low:

$| M_1 - M_{target}| < toll_{M1}$

For a tolerance of 5.0E-05 the iterative loop converges in about three or four iterations. At the end of the loop a new simulation has been done with a little bit different back pressure to verify the condition of UI. This simulation has the aim to check the inlet conditions and verify their independence from static back pressure. All this loop procedure has been implemented in a Matlab code in order to complete automatically the iterations.

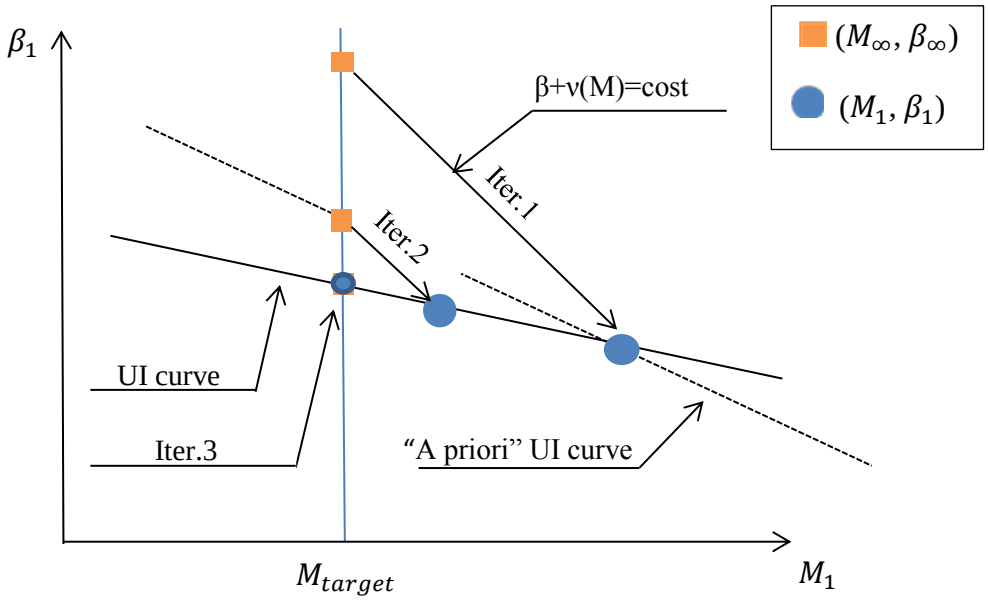

Figure 2.6: Procedure to achieve (M_∞, β_∞) with a specific M_1

2.2.1 Spill point pressure

At this point unique incidence inlet conditions have been founded in order to guarantee the desired inlet Mach target. Now a new iteration loop is going to be realized to reach the spill point; particularly the target of this new calculations is the static back pressure which realizes the condition explained by condition II of Figure(2.5), that specific pressure beyond which unique incidence is not right any more, and shock wave is detached from leading edge.

Practically this value has been founded increasing the initial low static back pressure step by step, until the inlet Mach number and flow direction were sufficiently far from the value of UI, a difference of 5.0*10E-04 appeared suitable. This situation is a clear consequence of overcoming the spill point pressure, and so this last pressure value and the last acceptable pressure value for UI existence represent the starting point for bisection method. So in the following attempt the static back pressure is the average value between the two. After the simulation with this average value two situation can occur:1) the inlet Mach number and flow direction are included in UI limits and so this pressure is the new lower value for bisection method; 2) the inlet Mach number and flow direction are beyond the limit hence this pressure represent the new upper value for bisection method. Proceeding with this method in a certain numbers of step the pressure range gets smaller and the process ends when the difference between the two pressure is lower than a fixed tolerance(for example 300Pa). All these points are illustrated in the following flow figure (where M_1 and β_1 indicates the values obtained after the simulation).

Also this loop has been implemented in a Matlab code which automatically realize these operations.

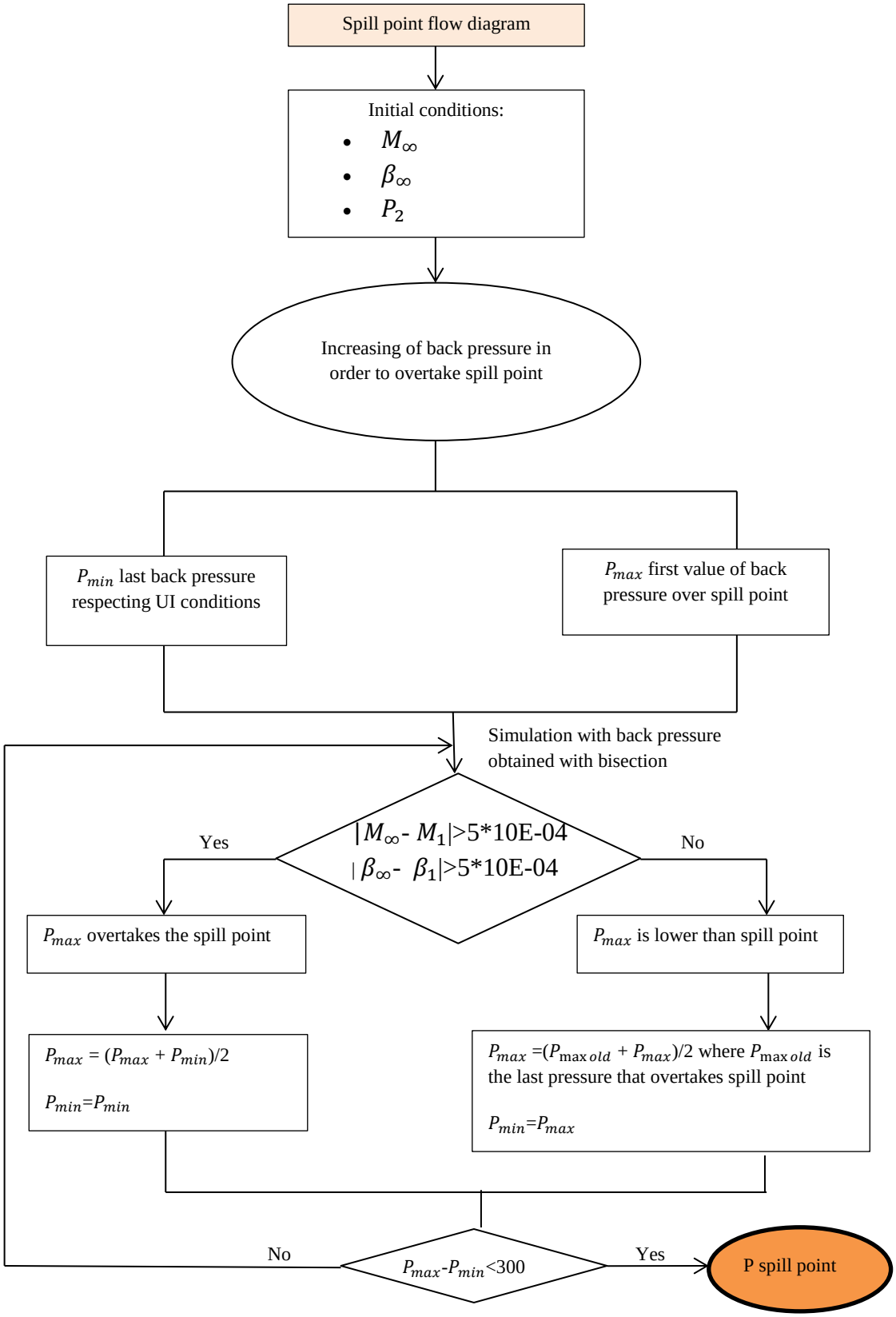

Figure 2.7: Spill point procedure

2.3 Cascade influence parameters

In this paragraph are exposed all the parameters that can affect the cascade performance.

2.3.1 Inlet Mach number influence

Transonic compressors realize great static pressure ratio applying a high rotational speed U, this involves an increasing of inlet Mach number: the higher inlet Mach number, the higher specific energy the compressor transfer. But this increasing in pressure ratio is not a free process, in fact as Figure(2.8) below shows, for Mach number range of 1.23 to 1.72, high inlet Mach number involve an increase also in total pressure losses.

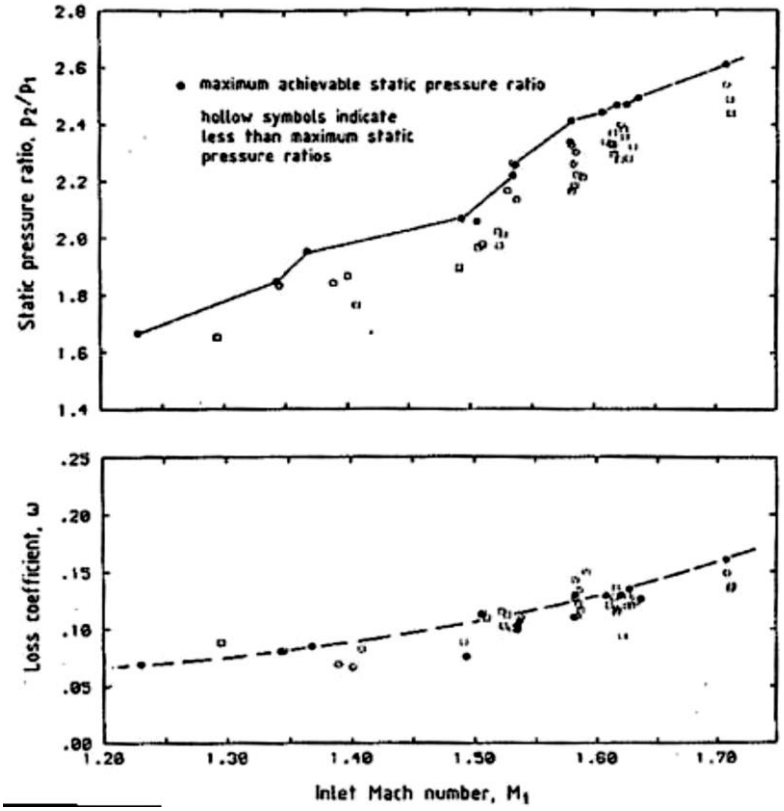

Figure 2.8: Influence of inlet Mach number on static pressure ratio and loss coefficient

2.3.2 Static back pressure

In UI conditions static back pressure doesn't influence the inner parameters, but it influences the shock wave pattern and its influence on losses. Increase back

pressure to high pressure ratios, generally produce a growth in losses; particularly shock loss reduces but increase viscous loss which is due to boundary layer separation. "The losses coefficient can be expected to be on the order of 0.10-0.15"[3]. Moreover for low static back pressure, exit Mach number shifts to supersonic values.

2.3.3 AVDR influence

The Axial Velocity Density Ratio is a parameter that measure the two-dimensionality of the flow. This is an important parameter because all simulations recreate a perfectly two-dimensional flow, while experimental tests are realized on cascades with a certain thickness so the flow can't be perfectly 2D, AVDR can tell how the experimental flow is far from the simulated one. Considering a meridional section of a compressor blade, AVDR can be calculated from continuity equation:

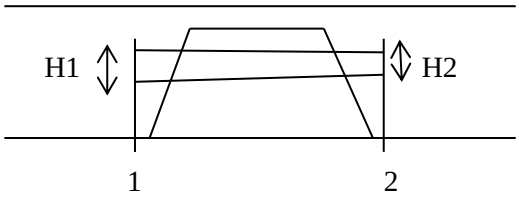

H $\rightarrow$ stream tube height
ρ $\rightarrow$ density
Cx$\rightarrow$ axial velocity

AVDR= $\frac{\rho_2 * C_{x2}}{\rho_1 * C_{x1}} = \frac{H1}{H2}$ (or sometimes AVDR=$\frac{H2}{H1}$)
Increase AVDR leads to an increasing of convergence flow, so reducing Mach number and consequently the losses correlated; this is more evident at higher pressure ratios where the stream tube convergence is more evident.
The AVDR influence on cascade flow has been analyzed by Tweedt ,Schreiber and Starken in [7]. The paper reports the variation of isentropic Mach number for a nominal inlet M=1.58 (β1=147.9°) an with constant pressure ratio.

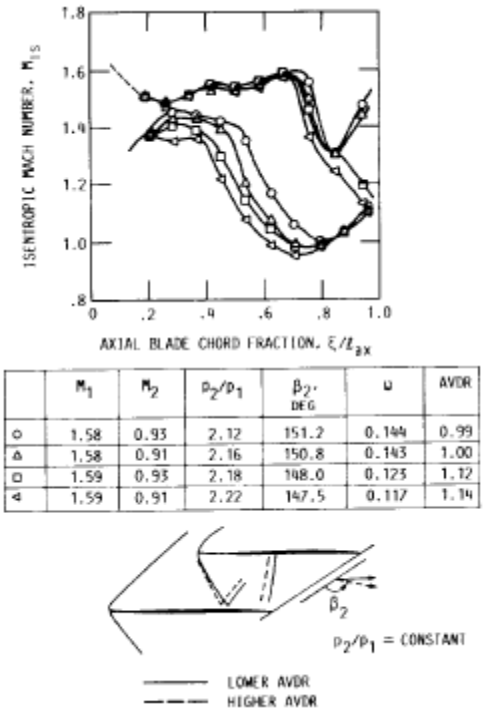

	M_1	M_2	p_2/p_1	β_2, DEG	ω	AVDR
○	1.58	0.93	2.12	151.2	0.144	0.99
△	1.58	0.91	2.16	150.8	0.143	1.00
□	1.59	0.93	2.18	148.0	0.125	1.12
◁	1.59	0.91	2.22	147.5	0.117	1.14

Figure 2.9: Influence of AVDR on the blade isentropic Mach number distribution[7]

"The main effect of increasing AVDR is a moderate upstream shifting of the rear passage shock waves and a slight steepening of the oblique shock waves at the passage entrance"[7], this behavior is shown in Figure(2.9) where the parametric curve with greater AVDR highlights a movement of the wave in the former zone of the blade. Moreover greater AVDR implies a reduction of loss, this in the case of high or moderate pressure ratios, the entity of loss reduction depends on the static pressure ratio how Figure(2.10) shows. At low and moderate pressure ratios an increase in AVDR causes increase in total-pressure losses. So if the condition at the exit of the cascade is of supersonic flow this second behavior appears. Instead if the flow at the exit is sonic or subsonic the behavior is opposite: an increase in AVDR involves a decrease in losses.

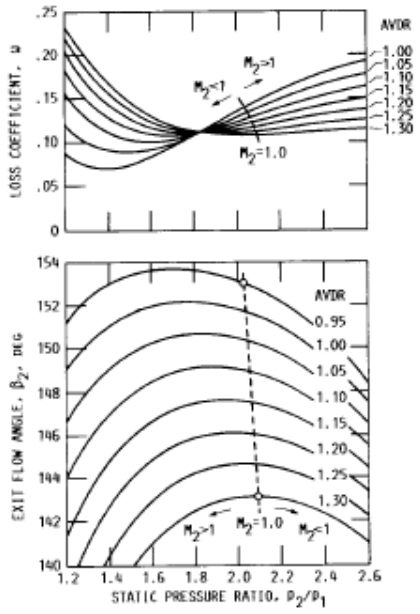

Figure 2.10: Influence of AVDR on loss coefficient and exit flow angle[7]

The figure above shows that AVDR influences also the exit flow angle: increasing AVDR reduces the exit flow angle and thereby increases the flow turning. The reason of this behavior is that maintaining constant pressure ratio requires that effective flow area remain constant, so the stream-tube contraction for higher AVDR necessitates the exit flow turn to smaller value. This particularly at low pressure ratios where the exit flow is supersonic.

2.4 Relation between linear cascade and rotor blade

All the tests and the simulations that have been considered in this work, involve cascade, so blades working in a two dimensional fluid domain. In "*Comparison of performance of supersonic blading cascade and in compressor rotors"* Mikolajczak et *al.*[8] investigated how the results obtained in this kind of tests can be useful for design of 3D rotors. In this work three different geometry of blade have been tested in a wind tunnel considering linear cascade and compared with similar profiles in rotor blades. They considered "J" profile, circular arc (CA) and multiple circular arc(MCA) with same characteristics:

- Chord = 3.75in
- Camber angle = 10deg
- Inlet Mach number = 1.35
- Chord angle = 30deg

Figure (2.11) shows the experimental results obtained for the three blades where cascade results are represented with solid line, whereas rotor tests are represented with open symbol. The cascade operates in unique incidence conditions, in fact the incidence ,that in this case "is defined as difference between the tangent to the

blade's leading edge mean camber line and the relative air angle"[8], remain constant until pressure ratio reaches spill point condition. Also rotor incidence is rather constant in good agreement with cascade results, this is particularly true for CA and MCA blades at least for static back pressure near the spill point. The "J" blade shows a certain difference between the rotor and cascade incidence, perhaps this is due to an important discrepancy in AVDR for the two cases, highlighting the importance of this parameter. Moreover this paper demonstrates all the importance of AVDR also in turning angle and total pressure losses: the more similar is AVDR for cascade and rotor, the more similar are turning angle and pressure losses for different pressure ratios. Figure(2.11) shows also that cascade can operate with lower maximum pressure ratios than rotor.

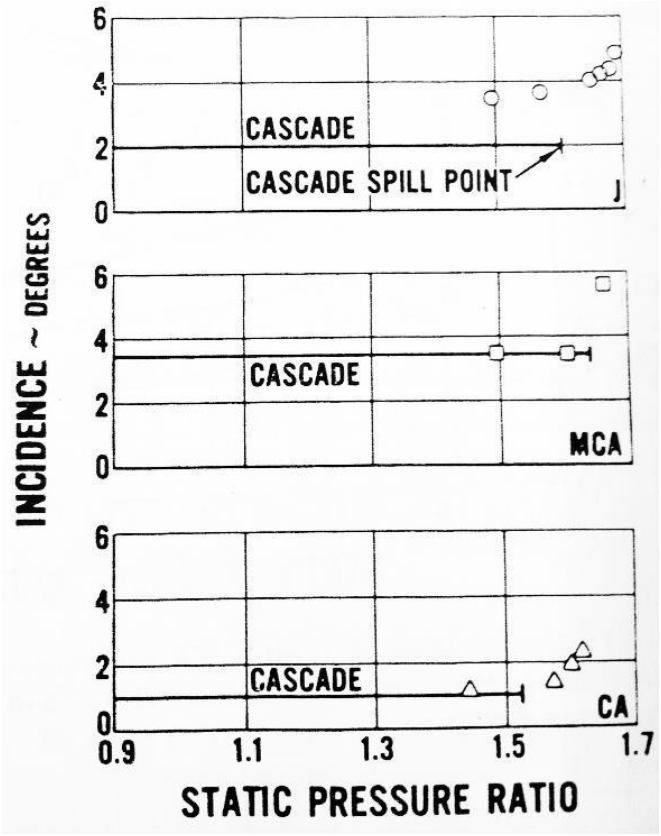

Figure 2.11: Incidence in function of static pressure ratio[8]

In conclusion 2D linear cascade are a convenient tool to obtain a better insight of the complex axial transonic compressor blade element and to realize a first investigation of rotor blade particularly for lower pressure ratios where the results are similar to the rotor ones.

3.Historical survey

In a compressor blade the mechanical energy can be transferred to the fluid substantially in three typologies of blade. From Euler's momentum equation $h=(U_2*c\theta_2-U_1*c\theta_1)$ the specific energy transferred is proportional to absolute flow turning this can be realized: 1)decelerating relative velocity, 2)turning relative velocity or 3)a mix of the first two. Hence all the blades influence the turning of the flow; the three typologies are: pure impulse cascade Figure(3.1), high turning supersonic reaction cascade and low turning supersonic reaction cascade Figure(3.2).

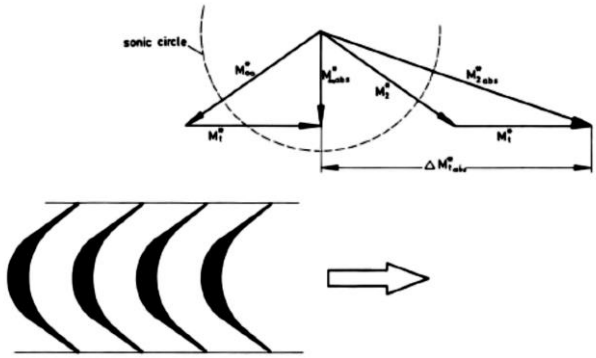

Figure 3.1: **Supersonic impulse cascade[9]**

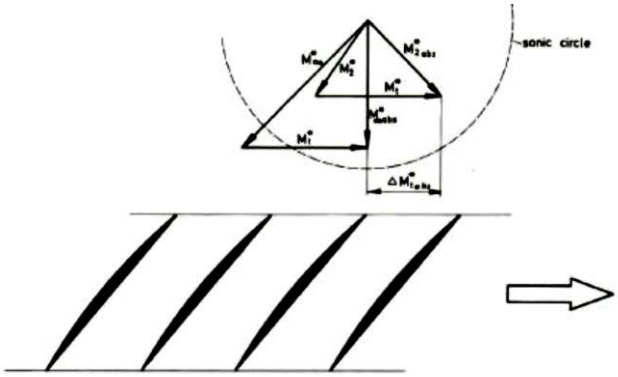

Figure 3.2: **Low turning supersonic reaction cascade[9]**

The figure above shows a pure impulse cascade, the mechanical energy of the rotor is transferred only into kinetic energy, without increasing of pressure, which is completely realized in the following stator at high supersonic velocities. In fact the relative velocity does not experience any change in his absolute value, but the flow undergoes to a high turning symmetrical to axial flow direction. This typology of energy transfer involves acceleration and deceleration with separation of boundary layer.

The figure below shows a typical shape of low turning supersonic reaction cascade, unlike the impulse cascade the velocity triangle highlights a very low turning and an evident deceleration of relative velocity through sound speed. The deceleration and consequently compression is realized in two phase: the first due to shock wave in the blade passage from leading edge, a second one due to deceleration of subsonic flow throw an increase of passage area.
The deflections imposed by the two parts are opposite in sign so they compensate each other, hence the turning is low. The limitations of this kind of blades lie in the instability of the throat area and the entropy rise for the first area, and separation of boundary layer connected with shock interaction for the second one.
All the blades that are going to be considered belong to low-turning cascade, in fact all of them generate compression with a first part of shock waves and a second compression realized on subsonic flow.

3.1 Evolution of compressor shape

The first rudimentary design of a compressor blade has been realized by Arthur Kantrowitz on the basis of his study on supersonic diffusers[3]. In the *"Supersonic axial-flow compressor"*[2] Kantrowitz theoretically shows that the waves which are primarily responsible for the high drag of isolated blade with supersonic Mach number can be eliminated in a cascade. The deign blade was joined with the idea of supersonic diffusers; so the blade passage was realized in order to reduce the passage area in the first part slowing down the velocity, till the deceleration through the speed of sound by a normal shock confined inside the passage. The further deceleration in the subsonic region has been realized increasing the passage area. This kind of blades realize the compression by the concept of *internal* compression ,where the only way to improve the rotor efficiency is to reduce the Mach number ahead of the normal shock wave and this have been realized increasing the thickness of the blades. Another reason of the great losses is that subsonic diffusion region diverged too rapidly with separation and strong interaction shock-boundary layer.
Some years later Creagh and Klapproth(1953)[10] and Lawrence and Melvin(1954)[11] introduced the concept of *external compression* in supersonic compressor blades. They proposed to use the spike diffuser(Oswatitsch[12]) principle for design of the inner part of the blades in order to achieve the isentropic contraction ratio. The spike diffuser allow the blades to produce a series of oblique compression waves ahead the passage entrance which contributes to reduce the Mach number before the normal shock where Mach reach the unity and the flow becomes subsonic. They also found that "the limiting contraction ratio was determined as function of the blade leading-edge wedge angle and the relative entrance Mach number"[10]. Figure (3.3) shows the design of external compression blade; the development of pre-compression waves is realized also by

the concave surface of suction side in the first part, which generates a series of compression waves that diffuse the flow.

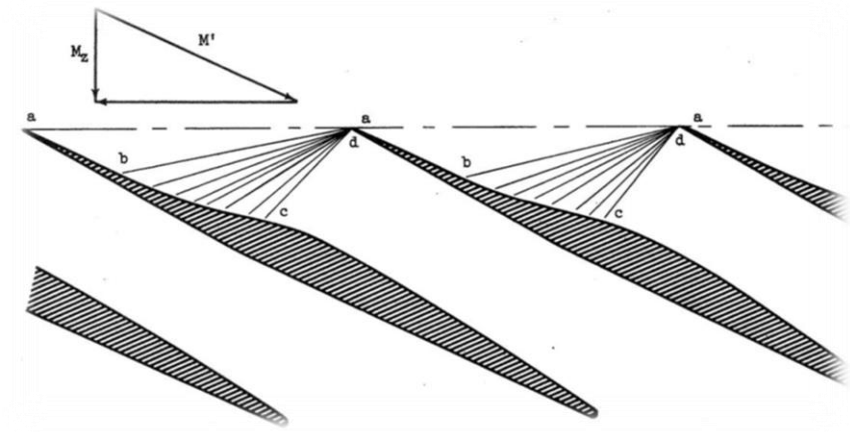

Figure 3.3: External compression in compressor cascade[10]

In the attempt to develop a design routine of transonic compressor blade it has been introduced the double circular arc theory(DCA). This theory defines the camberline as a circular arc composed of the same radius for both the supersonic and the subsonic part. The flow covering the suction surface passes through the convex curvature of the inlet part, this involve an acceleration of the flow, which is deflected by expansion waves. This acceleration can be tolerated till Mach number of 1.6 ahead of the shock, this means a maximum inlet Mach number of about 1.3.

To overcome the limits of double circular arc blades, Seyler and Smith (1967)[13] proposed a new blades' shape; in this blades the camberline consist of two circular arcs mutually tangent in the point where they join. The front arc is called supersonic arc, whereas the rear arc subsonic arc: this kind of blade has been called multiple-circular-arc(MCA). Usually is adopted a lower curvature arc in the front part to reduce acceleration and shock losses, and a greater one for the rear part. Comparison of DCA and MCA cascade has been realized by Mickolajczac in 1971 [8]; this highlights the improvement in pressure ratio Figure(2.11) (in fact the spill point pressure ratio of MCA blade is greater than CA spill point pressure ratio) and in efficiency that MCA cascade realizes than DCA cascade, which involves an excessive supersonic expansion deteriorating performance of cascade.

The successive shape blades have been realized trying to reduce the curvature of the entrance region and so realizing a system of compression waves directed to a reduction of Mach number ahead the normal wave. A new kind of profile has been proposed: the Circular-Wedge profile featured by a null curvature in the inner part so that it kept constant the Mach number up to the normal shock. A similar profile proposed has been the J-shape, which has similar characteristic of the previous.

Today the state of art of transonic compressors is the so called s-shape blade profile. This kind of blade belongs to low turning supersonic profile class and realizes the compression by the use of a series of pre-compression waves as is shown in the figure below:

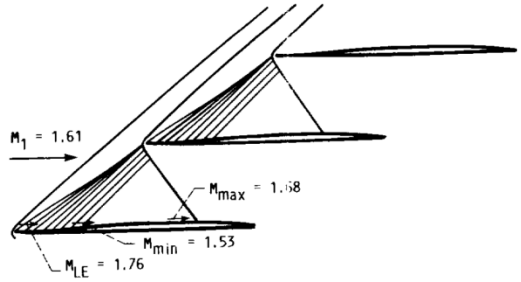

Figure 3.4: cascade design inlet wave pattern[14]

The finite thickness of the leading edge and the curvature of suction and pressure side generate a detached bow wave. This is a normal wave very close to the leading edge; downstream two oblique shock wave groups depart: one composed by expansion waves that remain in front of the blade (referred to as a "weak wave" as the expansion taking place is almost isentropic); and a stronger one that runs into the covered passage. As Figure(3.4) shows, the inlet Mach number increases in the first portion of suction side from 1.61 to 1.76 due to expansion waves; then the train of pre-compression waves reduces the flow velocity to a Mach number of 1.53. In the mid portion of the blade the curvature transits from concave to convex and this involves an acceleration of the flow before it encounters the shock system close to the profile wall of the suction side..

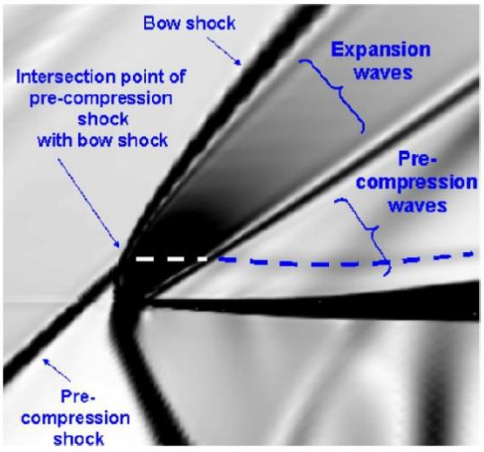

Figure 3.5: Schlieren picture of leading edge[15]

Here, the shock system is extremely complicated and generates the so called *lambda-shock system* . This is composed by a first oblique shock and a strong rear curved oblique shock, the oblique shock reaches a level so great that Mach

reflection is impossible and near the suction surface a quasi-normal shock appears, whose interaction with boundary-layer gives rise to a lambda-shaped shock . As for the suction surface, the pressure side shows an acceleration of the flow in the first part where the convex curvature supports this behavior and then after a quasi-normal shock the flow becomes subsonic.

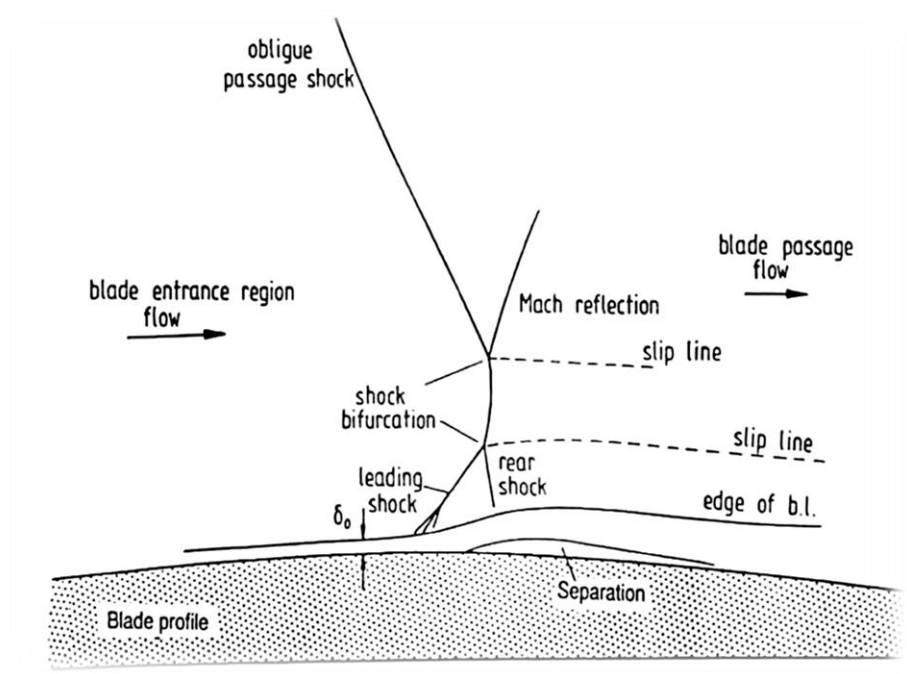

Figure 3.6:Flow structure of strong interaction in blade passage[14]

4. Kantrowitz blade

Let's start the study of the various transonic compressor blades, with the aim of try of understanding the specific physical phenomena that happens during the compression of the flow in these kind of blades. This study starts from the first transonic blade, that is the one designed by Arthur Kantrowitz on the basis of supersonic diffusers and on the basis of his study on supersonic cascade losses[2].

4.1 Airfoil and cascade geometry

One of the first tests[16] on a compressor rotor with a mass flow for 16-inch-diameter (0.4m) of about 28.5 pound per second (10.5 kg/s), shows still the great importance of the losses; the compressor rotor designed for a compressor ratio of 2.9, during the test has realized a pressure ratio of only 1.8 with 83 percent of rotor efficiency. However the advantages that this machine promised of being more compact by a factor of 4 than a comparable one (for the same compression ratio), led the improvements necessary to make it competitive.
This blade belongs to inner compression so the deceleration of the flow occurs by a normal shock that happens in the passage without pre-compression waves. The only way to reduce the Mach number ahead of the shock is to reduce the passage area and so decelerate the flow. This elementary way to compress the flow and the importance of normal shock strength justifies such a relatively low efficiency.
In order to test the Kantrowitz airfoil authors realized a cascade test before testing the compressor rotor to set-up the complex wave patterns which occurred in the transonic region. This static model had been realized with test conditions similar to compressor operation. The flow enters the cascade parallel to the suction side at the leading edge, and axial- flow Mach number is subsonic: entering Mach number is 1.6, stagger angle $\beta=60°$, the exit Mach number of about 0.6 and turning flow about 8.8° . The test is realized at spill-point, so no effect due to back-pressure is observed outside the model until such back pressure had been increased sufficiently to force the shock outside the model passage.
Blade's characteristics are presented in the figure below:

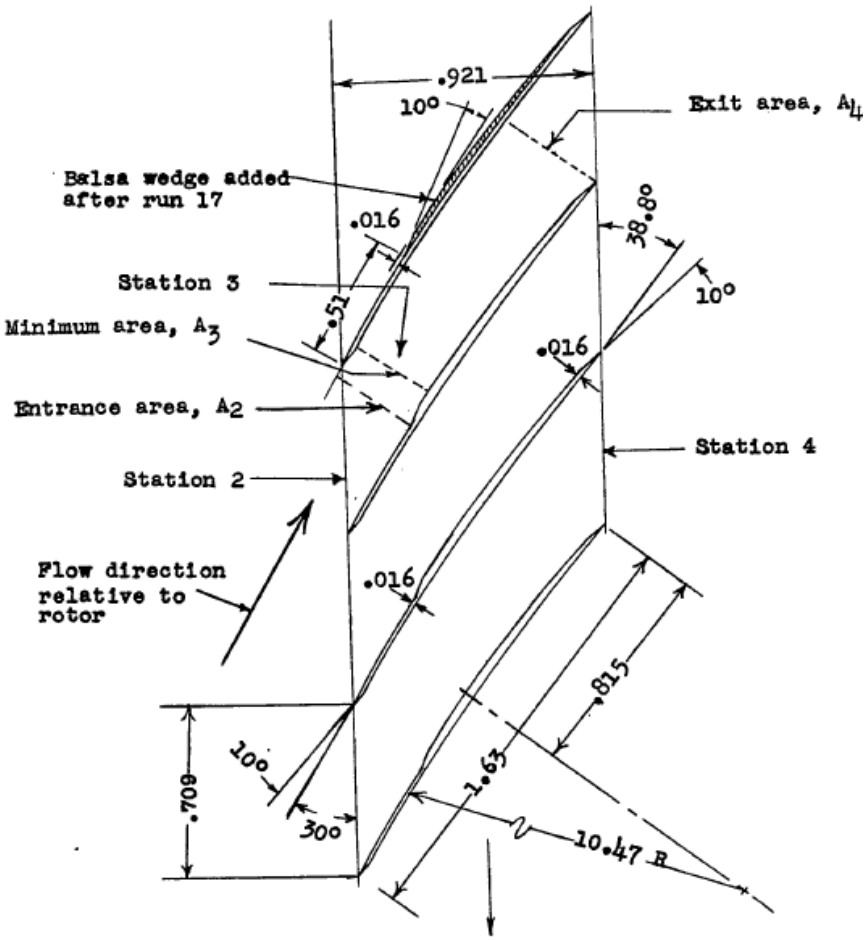

Figure 4.1: Kantrowitz blade design parameters[16]

Authors of experimental tests still remember that the supersonic diffusers insisted on the blade passage parameters and the blade shape is a consequence of these values. In particular they defined a contraction ratio as CR=$\frac{A_2}{A_3}$ and an expansion ratio as ER=$\frac{A_4}{A_2}$; by varying these two parameters they changed the blade shape.

As Figure(4.1) shows blade shape is composed by a straight thin profile with a balsa wedge attached on the suction side; the tests have been conducted with two contraction ratio and several values of expansion ratio. To increase the contraction ratio the wedge attached has been increased, and similarly for the expansion ratio. As shown below in Figure(4.3) the tests highlights an increase in boundary-layer separation with an increase of expansion ratio, and consequently a lower total pressure recovery. The separation reduces the effective expansion ratio at the trailing edge, obtaining at higher exit Mach number. On the other hand an increase in contraction ratio appears desirable because it increases shock efficiency and so the total pressure recovery even if it implies a lowest inlet Mach number.

The simulations have been led with a solid model realized with SolidWorks 12 using the dimensions of Figure(4.1) for the straight profile and changing the balsa wedge thickness from that indicated in figure in order to reach the CR used by the

authors in the report (CR=1.042) and an expansion ratio ER=1.15, with a leading edge radius spacing of $\frac{r_{LE}}{C}$=0.0005 (where c indicates the chord). The cascade features a chord value of c=41.4mm and a pitch of p=18mm.

4.2Flow solver and computational domain

After the realization of the solid model has been realized the computational grid necessary to the successive CFD solver.
The grid has been carried out using ANSYS® ICEM that is a powerful tool for structured grids. The structure is a multiblock grid with one O-grid around the blade, the location of the inlet face has been positioned 1.5*chord ahead the leading edge while the outlet face at 2*chord from the trailing edge in order to capture correctly the exit flow. A structured mesh is composed by a series of rectangular elements all connected each other; a good structured mesh (that is a mesh which correctly capture the flow) should have the rectangle's angles as similar as possible to 90 degrees, it should have adjacent rectangular of similar dimension, an important number of cells near the blade in order to capture the boundary layer. Moreover the mesh must verify the condition of periodicity, which means that in correspondence of the mesh border, the nodes of the successive mesh must be attached to the previous respecting the continuity. Because of periodicity the number and distribution of nodes of corresponding sides of the mesh must be equal and also the length of the block's side must be equal. The number of nodes that compose the mesh should not be neither excessive because the computational count would be too onerous, not too small in order to correctly understand the flow domain. The figure below shows the blocking structure: the form of the blocks and the consequent line of the mesh have been composed in this way to better respect the conditions listed above, moreover for the border nodes have been fixed the condition of periodicity fixing a value equal to the pitch to respect the periodicity. The density of the nodes is intensified in the proximity of the blade where are concentrated all the more interesting phenomena that involves the compressor; particularly in the zone immediately ahead the blade, at the leading edge, and in the front part of the blade passage where establishes the shock wave phenomena. The distribution of the nodes is summarized in the table below :

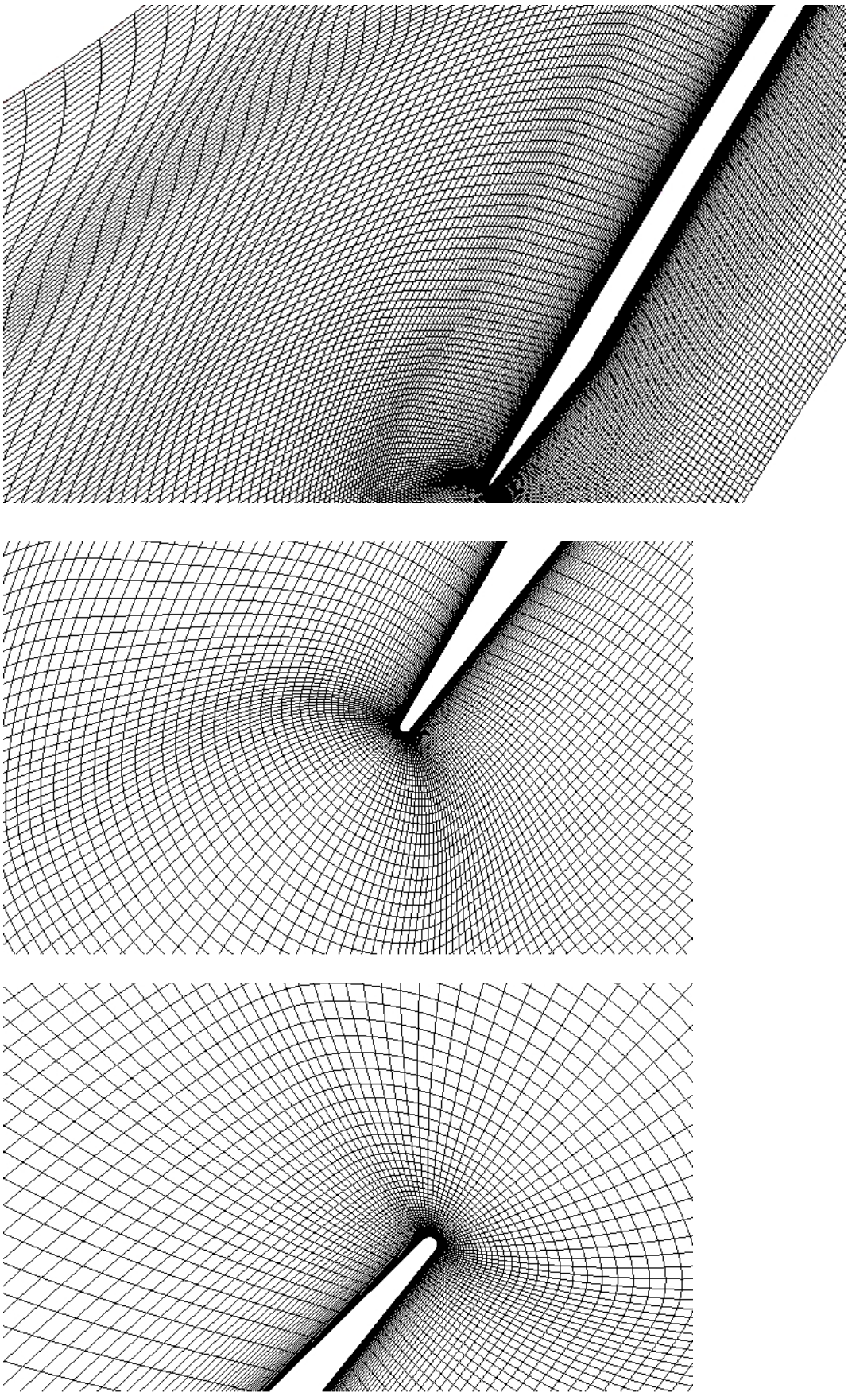

Figure 4.2: **Mesh structure front zone (first), LE (second), TE (third)**

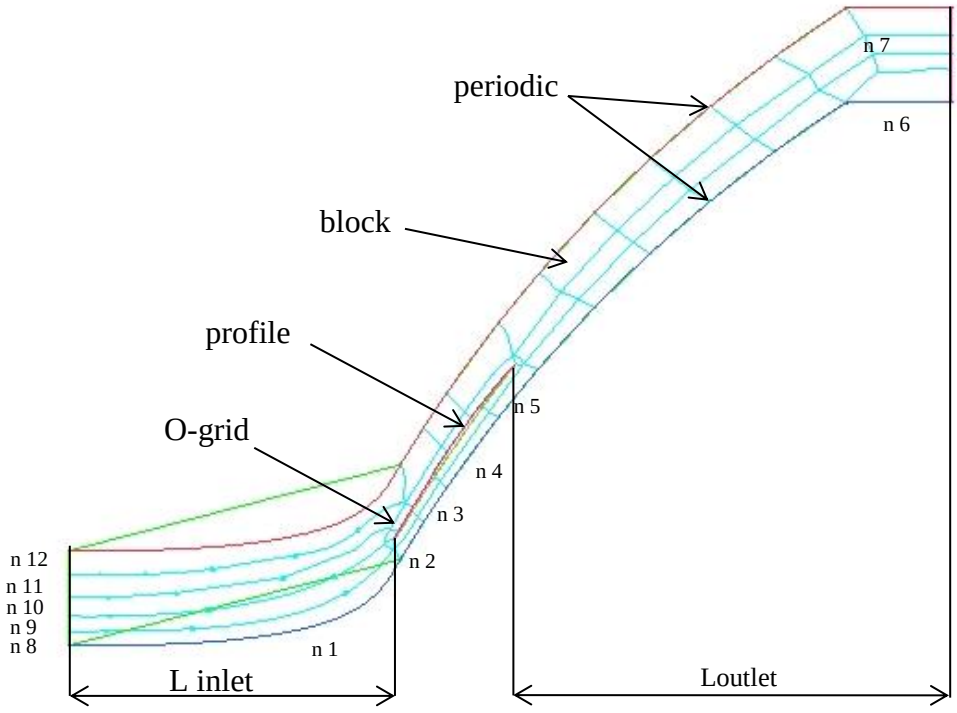

Figure 4.3: Blocking structure of Kantrowitz blade

Variable description	Variable	Nodes
Inlet	n 1	100
PS front zone	n 2	90
PS middle1	n 3	45
PS middle2	n 4	81
PS rear zone	n 5	80
Outlet	n 6	27
Trailing edge	n 7	30
Inlet lower zone	n 8	20
Leading edge	n 9	33
SS front zone	n 10	40
SS middle	n 11	37
Inlet upper zone	n 12	39
O-grid layers		67
O-grid growth rate		1.15
O-grid first layer		0.0007

When the blocking geometry has been completed and the number of nodes and their distribution on the blocking line has been fixed, the mesh has been converted in unstructured mesh and the smoothed using the following command:

- Number of iteration on surface: 10
- Smooth type on surface: Laplace
- Freeze options: selected parts

- Smooth along curves: None

The operation of smoothing is very important and delicate because modifies the mesh line in a way that could make the mesh of good or low quality.
ICEM provides also a series of parameters that give an indication of the quality of the mesh and particularly all the parameters above mentioned. The first parameter that the program returns after the smoothing process is the mesh *quality* which indicates how the mesh is distorced and so how the rectangular forms are far from perfect rectangles. The second important parameter is the *aspect ratio:* this parameter indicates the difference in dimension of the short and the long side of the rectangle, this because a great difference between the two dimensions is not tollerate for a mesh of good quality. This parameter is in contrast with another one: the *y+* which is dicussed below ,this requires a low value of the thickness of the first layer, and clearly this condition creates a great difference between the two sides of the rectangle. Finally another parameter which indicates the distortion of the mesh and considered here is the *skew* angle.The table below shows the values of these parameters:

Grid quality	min	max
Quality	0.5	1
Aspect ratio	0.004	1
skew	0.2	1

The general quality of the mesh can be considered good and this mesh is ready to be used by the flow solver Fluent.

Now the grid is ready to be imported in the computational solver ANSYS® Fluent v14 in which the Reynolds Average Navier Stokes (RANS) equations coupled with a turbulence model are solved adopting the finite volume method approach. The simulations have been carried out in two-dimensional steady state flow domain, for a fully turbulent compressible ideal gas in double precision.
Herein are listed the set-up characteristics of the flow solver: the first operation consists in scaling the mesh from meters to millimeters and setting on pressure-based. The next pass is to set-up the turbulence model:

- Energy on
- K-w SST

Fluid material:

- air
- density: ideal gas
- Cp: constant=1009.4[J/Kg*K]

Boundary Conditions at inlet:

- Pressure-far-field
- Static pressure: 24554[Pa]
- Mach number: 1.58
- X-component of flow direction: 0.5

- Y-component of flow direction: 0.866
- Turbulence method: Intensity and hydraulic diameter
- Turbulence intensity: 5%
- Hydraulic diameter: 0.01
- Temperature: 363[K]

Boundary conditions at outlet:

- Static pressure: 50000[Pa] (for the first attempt to find UI conditions)
- Turbulent method: Intensity and viscosity ratio
- Backflow turbulent intensity: 5%
- Backflow turbulent viscosity ratio: 10
- Backflow total temperature: 544.26[K]

The solution set-up has been changed during the simulations in order to get an easier convergence: the first part of the simulation has been conducted with coupled scheme, gradient scheme Green-Gauss Cell based and setting all the other derivative on the first order (Pressure, Density, Momentum, Turbulent kinetic energy, Dissipation rate and Energy). The solution controls have been fixed initially: flow courant number 20, Relaxation factor Momentum 0.45 and pressure 0.45. Particularly the solution controls have been fixed this values only for few iterations, then have been changed in: flow courant number 50, Relaxation factor Momentum 0.5 and pressure 0.5, till the convergence of the first order derivative.
When the simulation reaches the convergence in these conditions the derivatives have been switched on the second order; also in this case solution controls have been fixed initially on lower values in order to simplify the convergence and then fixed with the following values: flow courant number 30, Relaxation factor Momentum 0.45 and pressure 0.45. The convergence has been established when all residuals go under 1e-05. The flow has been initialized first with an hybrid initialization and then with fmg-initialization.

4.3 Results and validation

The survey of simulation results has been calculated with a *mass-weighted average* surface integral for the quantity of interest: static pressure at inlet and outlet surface and also for Mach number and velocity angle at inlet surface. For the total pressure the survey has been calculated with an *area-weighted average* surface integral. Moreover particular attention has been focused on the y+ parameter, this is important in order to keep valid the turbulence model near the wall (blade), so it is affected primarily by the first layer cells in contact with the surface blade. For the all the simulation it has been kept $y+<1$ that is a good value for a reliable simulation.
All the previous set-up characteristics have been fixed in order to better simulate the experimental tests descripted in [16]. Particularly the tests results have been reported at spill point conditions; so the aim of the simulations has been of

recreating that conditions. Hence it has been necessary to realize the UI control loop and spill point control loop described in 2.3 and 2.3.1, the first to find the UI conditions for the model realized and the second to find the spill point back pressure. As described above a low back pressure (50000[Pa]) has been initially imposed to find the UI conditions and for the second part the pressure has been increased step by step in order to reach the spill point pressure.
In the figure below are compared the results obtained with numerical simulations with the tests results at spill point conditions in order to validate the numerical model. Here are represented three curves: 1) the calculated total pressure recovery, but the authors themselves advise that this value is correct only when total pressure is uniform on the entire exit area, otherwise the calculated value would always be too low than the real one.2) Measured total pressure, but also in this situation the obtained value is too high than the real value because of the imperfection of the experimental apparatus ("no total pressure tubes were situated deep in the boundary layer"). 3) Model exit Mach number.
Hence the actual total pressure lies between the upper value given by measured total pressure and the lower of the calculated one.

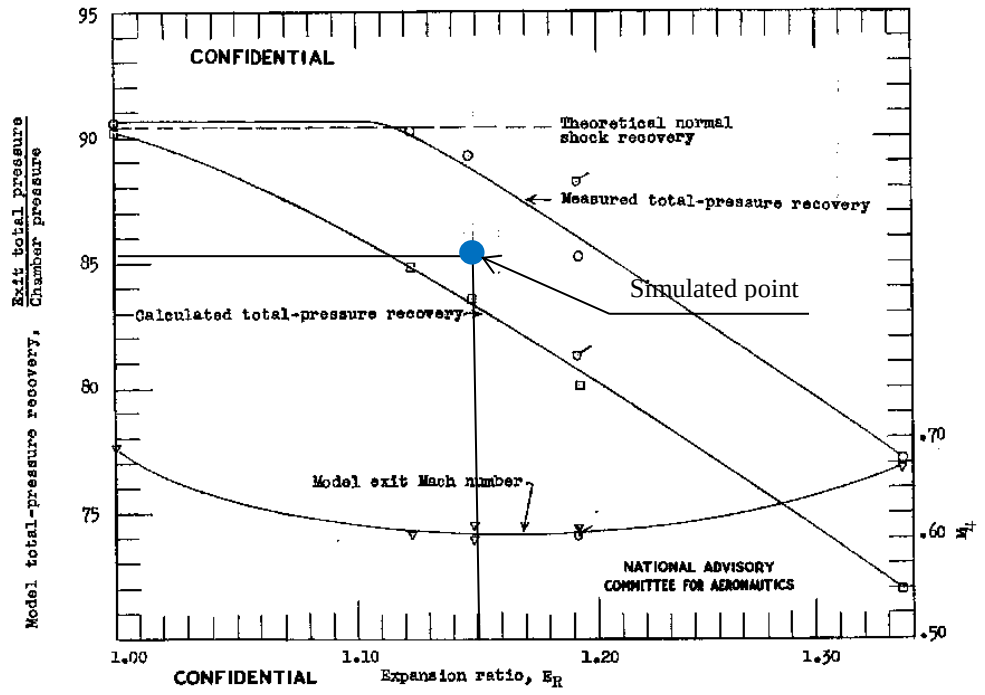

Figure 4.4 : Experimental results of Kantrowitz blade[16]

With the blue point is shown the result of numerical simulation obtained for a CR=1.042 and ER=1.15. The value of $\frac{Exit\ total\ pressure}{chamber\ pressure}$=0.853 (where chamber pressure is the inlet pressure), confirm the consideration before mentioned that the real value of exit total pressure is enclosed by the two curves. Moreover the exit Mach number assumes value of 0.68, this is a little bit greater than the measured

one, probably this is due to the great separation that occurs at the outlet, reducing the effective outlet passage area and so increasing the velocity. However this report has been written at the beginning of the study on transonic compressors so it is also probably that the surveys are not so accurate, hence a certain discrepancy with the reported value can be tolerated.
The flow field can now be analyzed plotting the Mach number contours in order to better understand the phenomena that involve the blade.

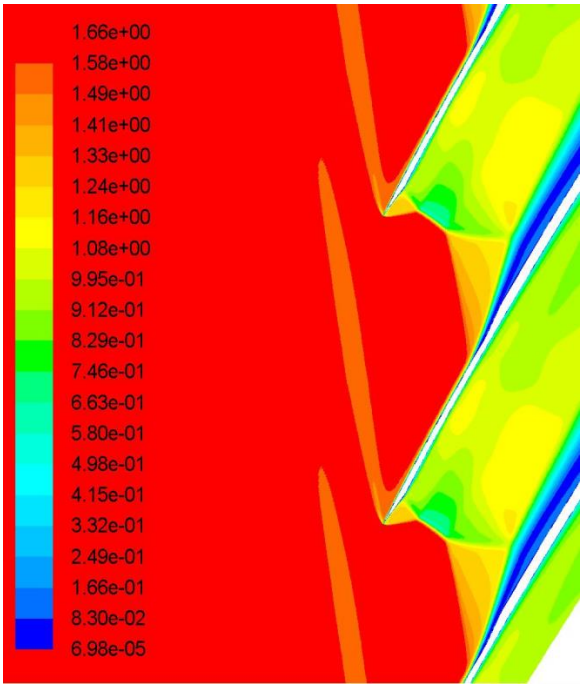

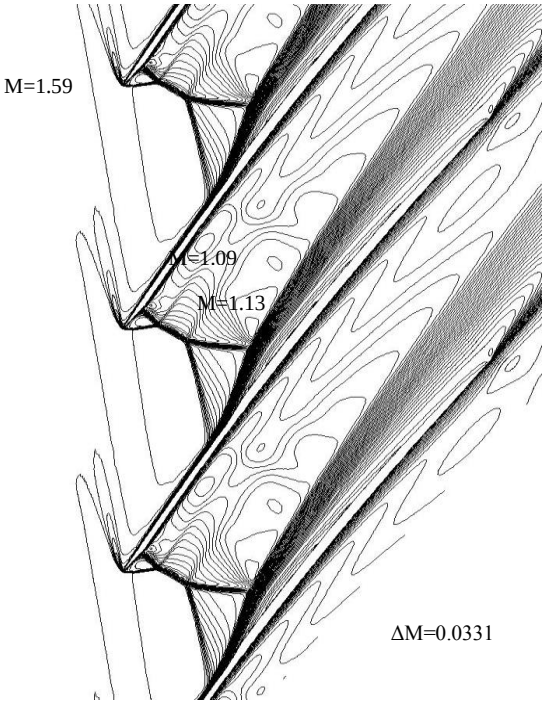

Figure 4.5: Mach number contours

As Figure(4.4) shows, the shock pattern is located at the entrance of the passage and the upper part of the shock wave is attached to the leading edge revealing a spill point situation. The flow approaches the blade with the imposed inlet Mach number=1.58, the leading edge of the blade encountering the flow generates an expansion wave which accelerates the velocity and deflects the flow, this follows the blade profile till the shock waves. The shock wave pattern is particularly complex: in the middle of the blade passage there is the formation of a normal dissipative shock, where the flow passes instantly from a supersonic Mach number to a subsonic one. In the zone immediately above the suction side there is a formation of a series of oblique compression waves which decelerate the flow progressively till a subsonic value. This phenomenon can be assimilated to the *lambda shock* of an S-shape airfoil, but in this situation the shock is strongly increased probably because of the great boundary-layer separation in the rear part of the blade. This could be also explained because "it has been observed that the lambda shock develops when the oblique shock passages impinges on a relatively strong convex curved part of the profile surface"[3] and in the blade former zone the profile is convex. In the upper part of the shock, on the pressure side, the local normal shock in correspondence of the leading edge attaches itself with the normal shock in the passage by a strong oblique shock, which decelerates the flow in the first zone of pressure side.

Then in the rear part of the blade the subsonic flow is subjected to a reacceleration of the flow due to a reduction of passage area because of separation of boundary-layer with a finally deceleration till the exit Mach number. Both this great separation and the strength of normal shock are the reasons of low efficiency, in fact:

Loss coefficient $\omega=\frac{p_{01}-p_{02}}{p_{01}-p_1}=0.2$

This great separation could be reduced and so realize a larger total-pressure recovery reducing the expansion ratio and increasing the contraction ratio[16]. In conclusion the problematic point of this blade could be summarized in the convex curvature of the fore zone of the blade which leads to the dissipative lambda shock and the distribution of passage area section which causes the great separation of the boundary-layer.

Seeing these results of great loss coefficient and strong separation this blade seems to be of low quality and without any utility for the aim of transonic compressors; but it is important considering that this is the first transonic blade ever created in history and that the authors yet didn't know the complexity of the phenomena involved in the compression process.

5. Double circular arc blade

Remarkable separation of the boundary layer and the high value of loss coefficient found in the Kantrowitz blade led to search for new geometries in order to increase the blade performances. Also the Double circular arc blade shape belongs to the *inner compression* blades, so all the compression process happens in the blade passage mainly by the use of a normal compression wave.

5.1 Airfoil and cascade geometry

The DCA blade consists in two circular arcs: one for the suction side and another for the pressure side; a simple scheme of a DCA a cascade is shown in Figure(5.1).

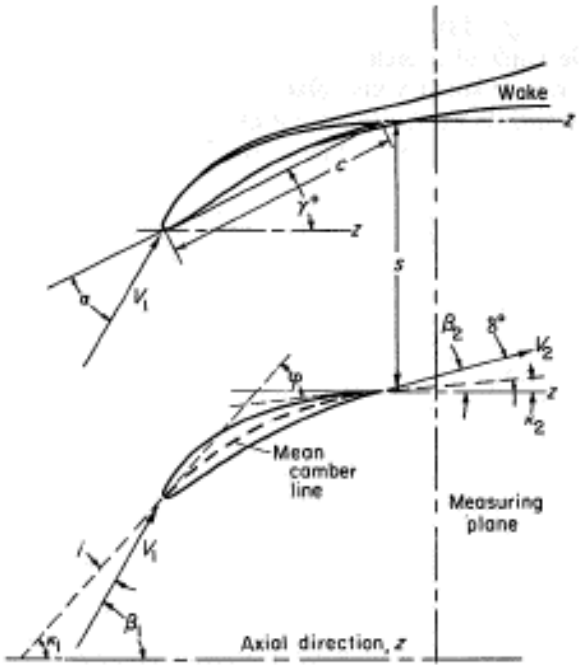

Figure 5.1: Double circular arc blade design

The figure above shows that this kind of blade is characterized by a former convex zone; such curvature involves an acceleration of the flow, which is deflected by expansion waves. Unlike the previous blade, in this one the throat area and so the compression takes place downstream in the chord length; in fact the normal shock takes place at a greater chord length. The blade geometry has been obtained from [8]; this paper documents a comparison between a supersonic cascade and a compressor rotor, although the thickness distribution of tested

blades (double circular arc, multiple circular arc and J-shape) are also reported. The most important blade characteristics are reported below:

- Chord length = 3.75 in
- Camber angle = 10 deg
- Inlet Mach number = 1.35
- Chord angle = 30 deg
- (blade spacing)/(chord) =0.8
- $(\text{thickness})/(\text{chord})_{max}$ = 0.044

The blade incidence was set by making use of concept of *unique incidence*, so in the experimental tests the difference between the flow angle at the entrance of the blade passage(β_1) and the flow angle far from the blade (β_∞), which verify the UI conditions, has been found and described.

In the numerical simulations, unique incidence conditions have been found for this specific blade with the UI control loop, as already explained in 2.3. Hence the spill point pressure has been found, because the experimental tests report the incidence variation associated with the static pressure ratio; so when the incidence changes its value, and the spill point pressure ratio has been exceeded, the spill point condition can be found.

All the parameters listed above permit to recreate the solid model of the cascade geometry.

5.2Flow solver and computational domain

Like the previous blade, the solid model has been imported in the meshing program ANSYS® ICEM in order to create the structured grid. Also this grid is composed by rectangular elements with the same rules listed above; particularly also this time a O-grid structure has been realized around the blade. The location of the inlet face has been positioned 1.5*chord ahead the leading edge while the outlet face at 2*chord from the trailing edge in order to capture correctly the exit flow. Another important characteristic, that also this time has been imposed, is the periodicity in order to join two consecutive blade mesh, this binds the length and the number of the nodes joined. The number of the nodes has been changed from the previous case in order to maintain the same mesh quality, in fact this blade was extremely different from the Kantrowitz ‘s one in dimensional terms(chord length about 95mm in this case, different from the previous which was about 41mm) and also the fluid domain geometry enclosing the blade is different. Also in this case the blocking structure has been realized in a way to respect very well all the conditions and the number of nodes has been decided in order to concentrate them in the more interesting zones(former zone, leading edge and trailing edge). The distribution is explained in the figure below:

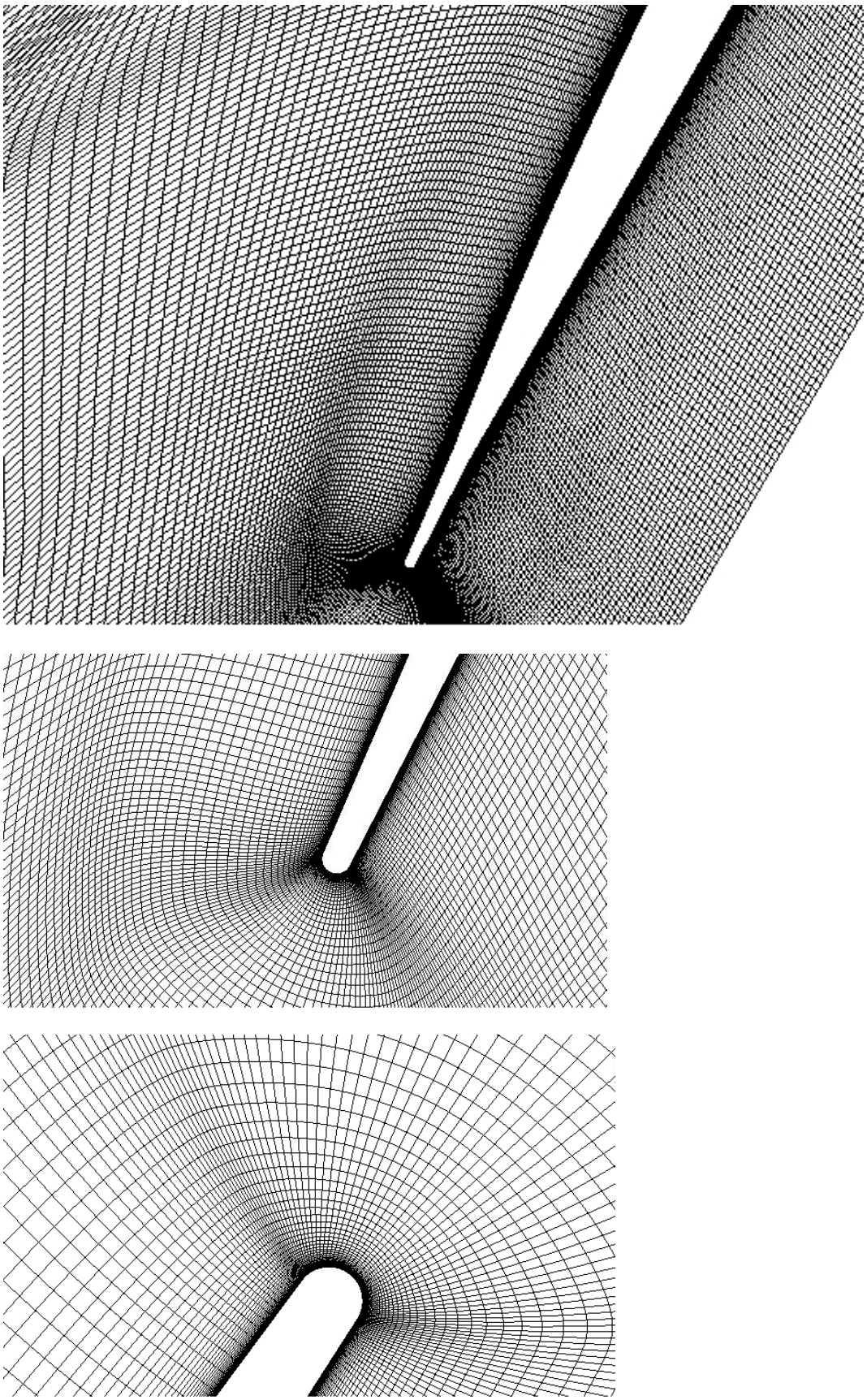

Figure 5.2: Mesh structure front zone (first), LE (second), TE (third)

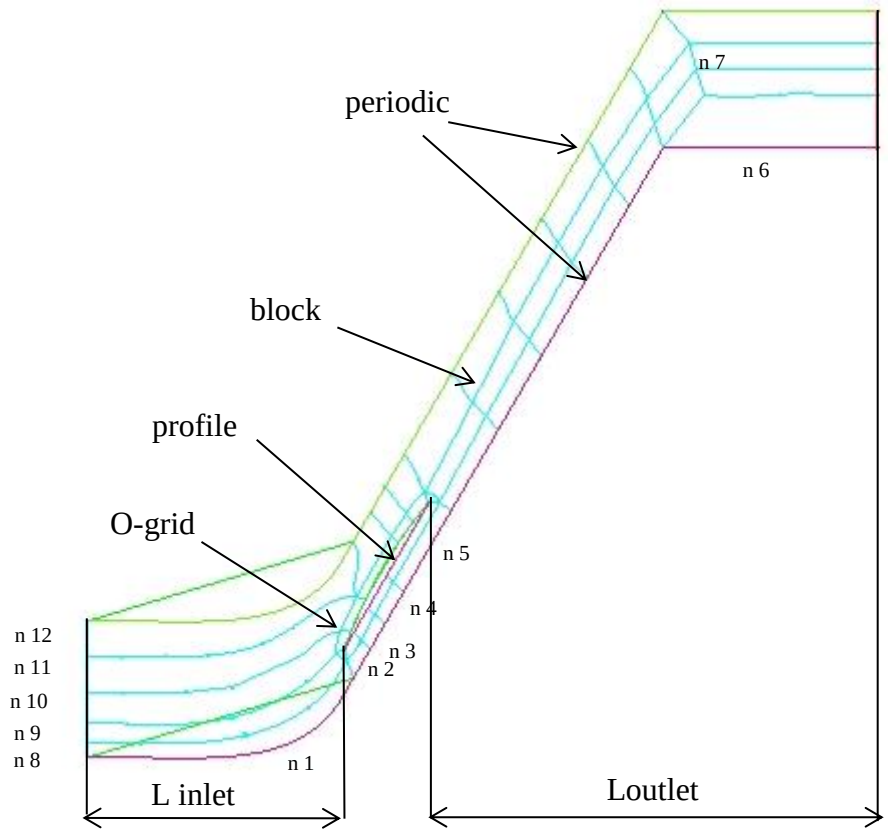

Figure 5.3: Blocking structure of DCA blade

Variable description	Variable	Nodes
Inlet	n 1	85
PS front zone	n 2	80
PS middle1	n 3	45
PS middle2	n 4	50
PS rear zone	n 5	125
Outlet	n 6	70
Trailing edge	n 7	50
Inlet lower zone	n 8	26
Leading edge	n 9	35
SS front zone	n 10	60
SS middle	n 11	45
Inlet upper zone	n 12	39
O-grid layers		67
O-grid growth rate		1.15
O-grid first layer		0.0004

The Figure(5.2) above shows a block distribution similar to the Kntrowitz blade, but not strictly the same, this because of a little difference in the fluid domain shape. Table above shows the nodes distributions, this is different from the precedent because of the different blocking structure. Also the O-grid first layer has been changed from 0.0007 to 0.0004 in order to reduce the value of y+.

Completed the nodes distribution, the mesh has been converted in unstructured mesh and smoothed using the following parameters:

- Number of iteration on surface: 10
- Smooth type on surface: Laplace
- Freeze options: selected parts
- Smooth along curves: None

Also this time to analyze the mesh quality the same three parameters have been calculated and examined: *quality*, *aspect ratio* and *skew*. The definition of these parameters is the same discussed in 4.2, the value for this type of mesh is reported in the table below:

Grid quality	min	max
Quality	0.5	1
Aspect ratio	0.001	1
skew	0.1	1

Aspect ratio and skew have a minimum value a little bit lower than the precedent blade but however the grid maintain a good quality and is ready to be simulated.

Also this time the computational solver used is ANSYS® Fluent v14, the mesh has been imported and simulated with a two-dimensional steady-state flow domain, for a fully turbulent compressible ideal gas in double precision.
The first step is to scale the mesh from meters to millimeters and fix the type solver on pressure-based. Now the second step is to define the turbulence model:

- Energy on
- K-w SST

Fluid material:

- air
- density: ideal gas
- Cp: constant=1009.4[J/Kg*K]

Boundary Conditions at inlet:

- Pressure-far-field
- Static pressure: 101325[Pa]
- Mach number: 1.35
- X-component of flow direction: 0.5
- Y-component of flow direction: 0.866
- Turbulence method: Intensity and hydraulic diameter
- Turbulence intensity: 5%
- Hydraulic diameter: 0.04
- Temperature: 399[K]

Boundary conditions at outlet:

- Static pressure:130000[Pa] (for the first attempt to find UI conditions)

- Turbulent method: Intensity and viscosity ratio
- Backflow turbulent intensity: 5%
- Backflow turbulent viscosity ratio: 10
- Backflow total temperature: 544.26[K]

The solutions step-up has been changed during the simulation in order to better reach the convergence: the solution scheme has been fixed on coupled for all simulations and the gradient scheme on Green-Gauss Cell Based. The other derivative parameters (Pressure, Density, Momentum, Turbulent kinetic energy, Dissipation rate and Energy) have been fixed on first order in order to favor the successive convergence of second order. The solution controls have been fixed as now described:

- Flow courant number = 20
- Relaxation factor momentum = 0.4
- Relaxation factor pressure = 0.35

This only for the first 150 iterations to support the convergence, then for the others has been changed in:

- Flow courant number = 50
- Relaxation factor momentum = 0.5
- Relaxation factor pressure = 0.5

These last values have been used also in the second part of the simulation, where the derivatives have been imposed on second order after reaching the convergence for the first order. The convergence has been established when all residuals go under 1e-05. The flow has been initialized first with an hybrid initialization and then with fmg-initialization.

5.3 Results and validation

At the end of the simulation the parameters magnitude have been calculated with a *mass-weighted average* surface integral for static pressure at inlet and outlet surface and also for Mach number and velocity angle at inlet surface. For the total pressure the survey has been calculated with *area-weighted average* surface integral. Another important parameter, as already said before, is the y+ which has been kept minor than 1 in order to keep valid the turbulence model.
Because the experimental tests reported in [8] have been realized at spill point conditions, the numerical simulations have been conducted in order to find the spill point pressure. Hence the static back pressure initially fixed on 130000[Pa] has been increased step by step as illustrated in 2.3.1, reaching finally the spill point pressure.

Figure(5.3) shows experimental results, compared with simulation results:

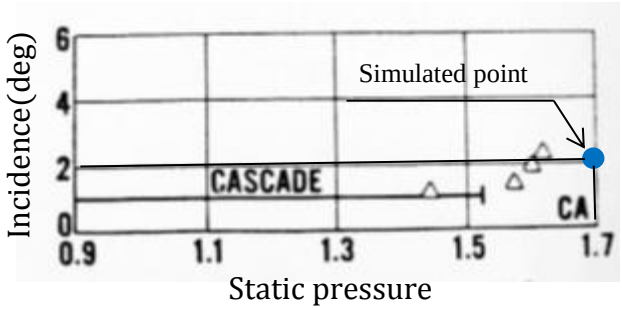

Figure 5.4: Experimental results for DCA blade[8]

This figure shows a certain difference between the two value, this is due to two important reasons: 1) the first is the substantial lack of information about the trailing and particularly leading edge geometry. This is fundamental in the UI conditions, in fact the flow angle β_1 is related with the inlet Mach number and the leading edge geometry; this explains the difference between the experimental and the numerical incidence (in this paper incidence is defined as the difference between the tangent to the blade's leading edge camber line and the relative air angle). 2) the difference in AVDR between numerical and experimental tests, as following shown this is a frequent reason in this kind of tests. In fact in the two-dimensional numerical flow domain the AVDR value is always equal to 1, this is in contrast with experimental tests where the AVDR is lower than 1, considering the case of spill point pressure ratio the AVDR assumes the value of 0.9 . This can explain the discrepancy in spill point pressure ratio, in fact a lower AVDR leads to shift upstream the shock wave and so the blade reach the spill point pressure ratio with a lower value of static back pressure. The interaction of these two phenomena can explain the gap between numerical test and experimental one.
The phenomena involving the blade flow field can be analyzed plotting the Mach number contours:

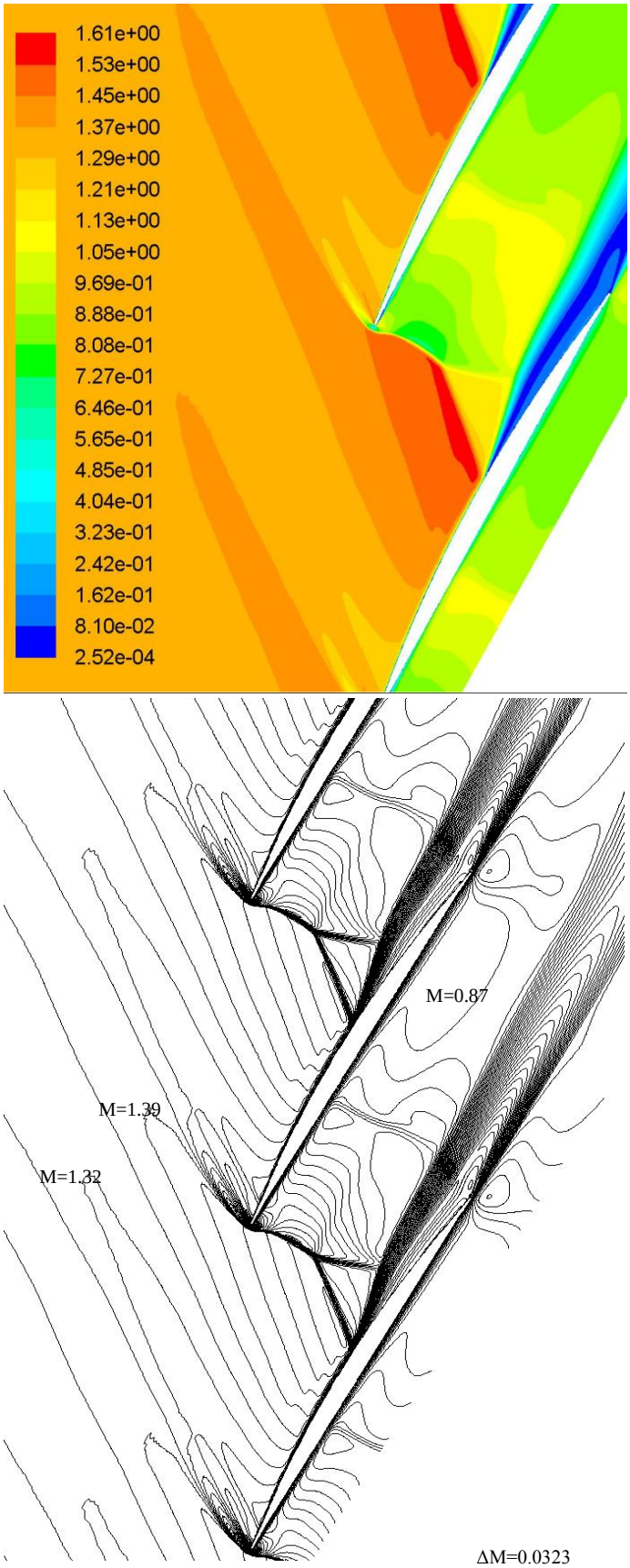

Figure 5.5: **Mach number contours**

As Figure(5.4) shows the wave structure is strictly similar to the previous blade, but with some interesting differences: the convex curvature of the former zone induces acceleration of the flow and the following expansion waves deflects the flow along the blade surface. Hence the successive wave structure is very similar to Kantrowitz blade; also this time the convex curvature generates a lambda shock where the flow is decelerated from supersonic to subsonic by a series of oblique compression waves. Above this lambda shock wave figure shows a quasi-normal shock which instantly pass the flow from supersonic to subsonic. These shock waves are attached to the local normal shock at the leading edge confirming the spill point situation. In the rear part of the blade the boundary layer presents a great separation which leads to an increase in losses. This separation is not so widespread along the chord length (because the shock is located more downstream than Kantrowitz blade) so this reduces in some way the entity of this kind of losses compared with the separation that occurs in the previous blade.

Also for this blade the loss coefficient is very high but however lower than the Kantowitz blade's one; this can be ascribed to the reduction of length of boundary-layer separation:

loss coefficient $\omega=\frac{p_{01}-p_{02}}{p_{01}-p_1}$ =0.18

The importance of lambda-shock and the severe boundary-layer separation can explain the greatness of loss coefficient.

In conclusion this blade has a fluid dynamic behavior similar to the Kantrowiz blade but with some adjustment particularly in the position of the shock in chord percentage and in shock-boundary layer interaction.

6.Multiple circular arc

The limitations that remained in double circular arc have been solved in part in Multiple Circular arc blade (MCA); this kind of blade consists in two circular arcs forming the suction surface and two circular arcs forming the pressure surface. In this way is possible to have a better control in shock loss and throat area than using a single circular arc; generally for the forward part has been used an arc with lower curvature than the arc in the rearward part. The reasons of this choice will be explained in this chapter.

6.2Airfoil and cascade geometry

As already said this kind of blade consists of two circular arc for the pressure side and two for the suction side. The profile geometry has been modelled from the blade coordinates reported in "V.4 TEST CASE E/CA-4, LOW SUPERSONIC COMPRESSOR CASCADE MCA"[17], here the profile coordinates are reported excluding the leading and trailing edge zone, which have been recreated in order to preserve the slope and the curvature of the profile in the connection point. The main characteristics of the blade and cascade geometry and test are listed below:

- Chord length = 90 mm
- Stagger angle = 138.51°
- Pitch chord ratio = 0.621
- Inlet Mach number = 1.086
- Inlet flow angle = 148.5°
- $p2_{\infty}/p1$ = 1.448
- AVDR = 1.184
- Re = 1.49*10E06
- $M2_{\infty}$ = 0.699
- $\beta 2_{\infty}$ = 135.2°;
- $pt2_{\infty}/pt1$ = 0.9561
- ω = 0.084

The test cascade has been conducted at spill point condition, so to validate the numerical model, also this has been simulated at spill point conditions. Also this time has been implemented the Matlab loop to find the UI conditions first and then the spill point pressure ratio. It is worth notice that because of a little different leading edge geometry between the test case and the recreated model, the UI conditions are a little bit different and so also the inlet flow angle.
The figure below shows a scheme of the cascade geometry with all its parameters:

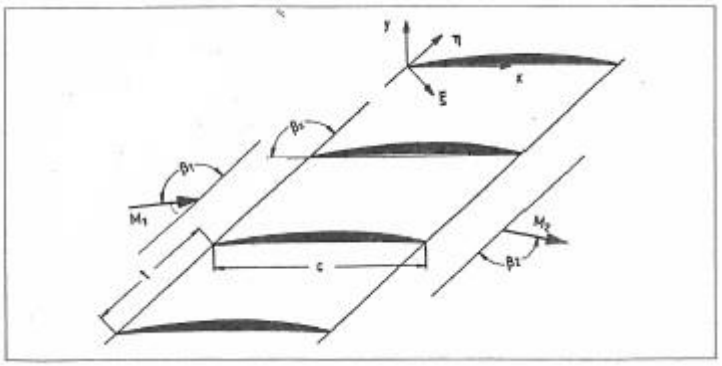

Figure 6.1: MCA blade design[17]

6.2Flow solver and computational domain

The second step is to realize the grid geometry also this time with ANSYS® ICEM to create a structured mesh. The blocking is similar to the precedent one because the blade geometry is dimensional near to the DCA blade. Also this present an O-grid around the blade and the inlet zone is located at 1.5*chord and the outlet at 2*chord to better capture the outlet flow. Also this time has been imposed the periodicity in order to join two blade passage fixing in this way the length and the nodes number of the two sides of the mesh. The mesh nodes number and distribution have been decided in order to better analyze the flow and so concentrate the majority of them in the more critical zone(former zone, leading edge and trailing edge). The blocking structure and nodes distribution are shown in Figure(6.2):

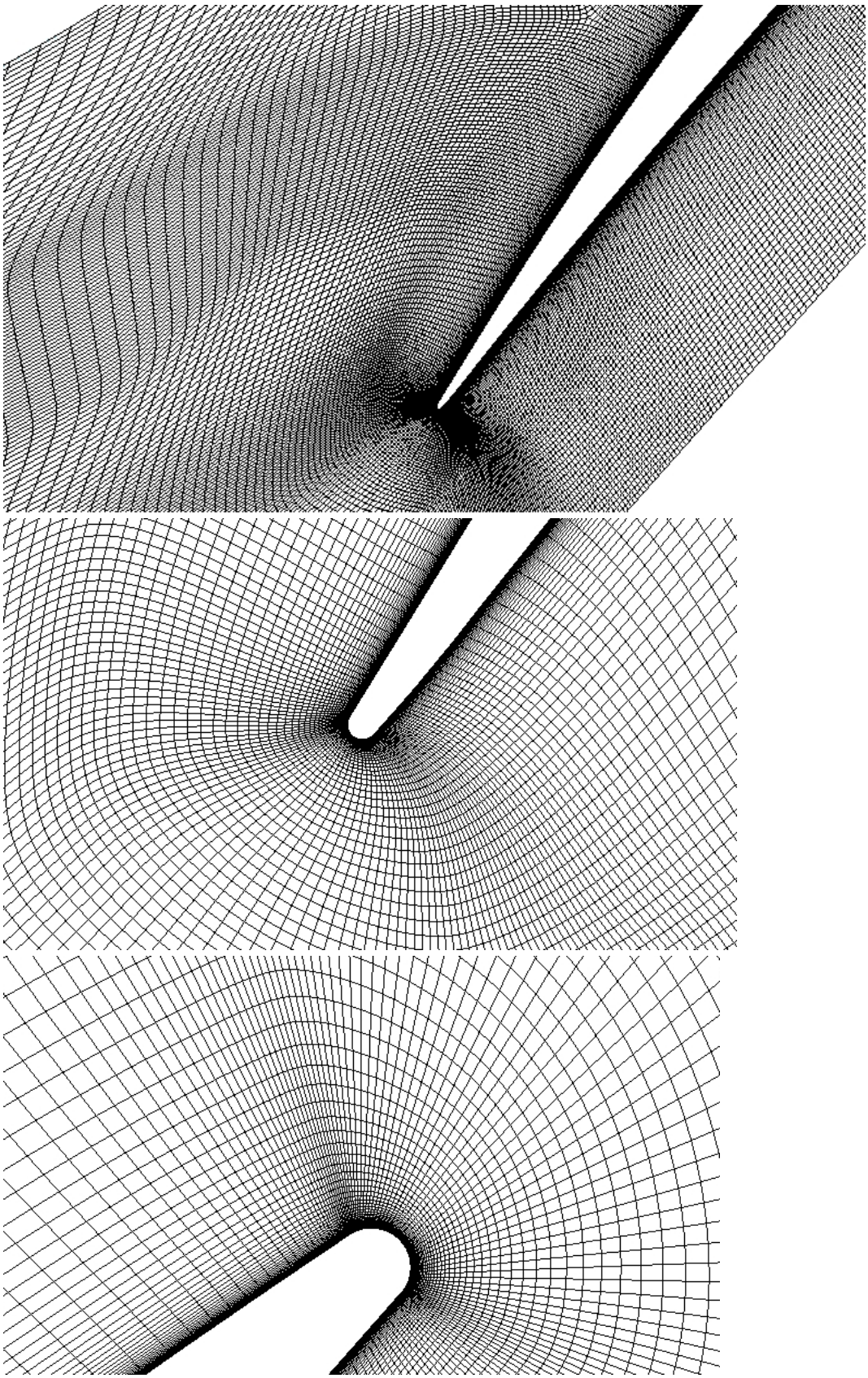

Figure 6.2: **Mesh structure front zone (first), LE (second), TE (third)**

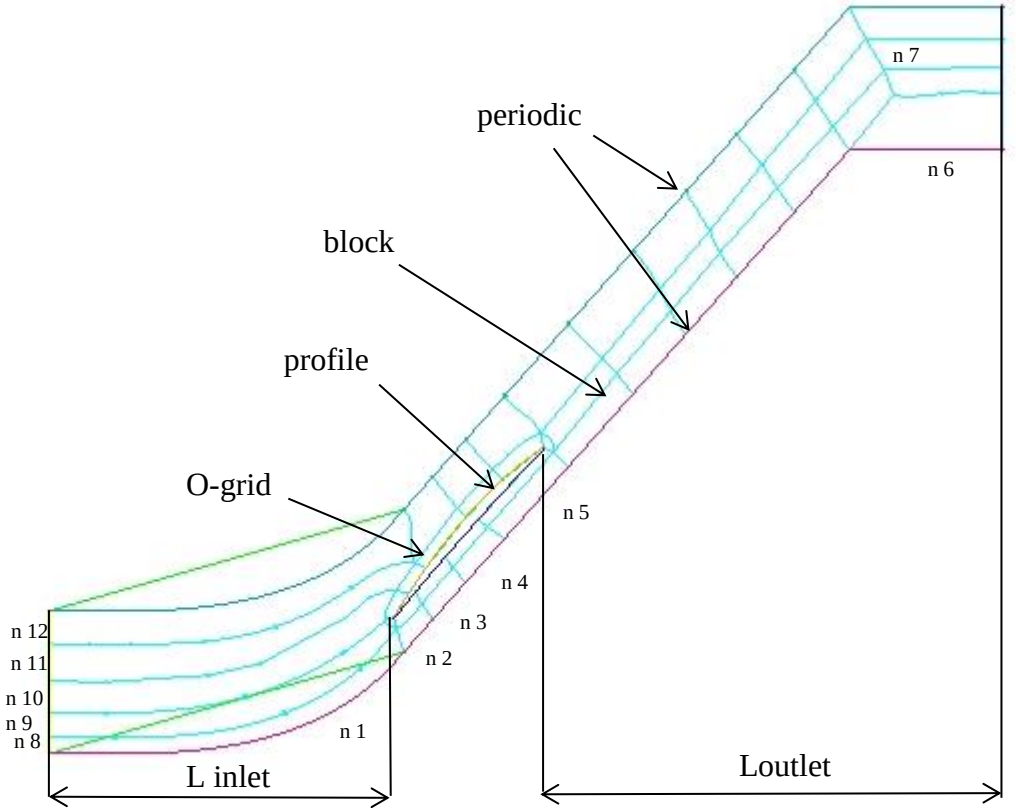

Figure 6.3: Blocking structure of MCA blade

Variable description	Variable	Nodes
Inlet	n 1	85
PS front zone	n 2	80
PS middle1	n 3	45
PS middle2	n 4	65
PS rear zone	n 5	125
Outlet	n 6	35
Trailing edge	n 7	50
Inlet lower zone	n 8	26
Leading edge	n 9	35
SS front zone	n 10	60
SS middle	n 11	45
Inlet upper zone	n 12	39
O-grid layers		67
O-grid growth rate		1.15
O-grid first layer		0.0004

From this table is clear that the mesh structure and the nodes distribution is substantially the same of DCA blade.

Completed the nodes distribution, the mesh has been converted in unstructured mesh and smoothed using the following parameters:

- Number of iteration on surface: 10

- Smooth type on surface: Laplace
- Freeze options: selected parts
- Smooth along curves: None

The same parameters of the previous blades has been checked to verify the goodness of the mesh: *quality*, *aspect ratio* and *skew*. The definition of these parameters is the same discussed in 4.2, the values for this type of mesh is reported in the table below:

Grid quality	min	max
Quality	0.5	1
Aspect ratio	0.001	1
skew	0.25	1

As the table before shows the grid quality is very good and it can be used in the flow solver to analyze the flow distribution.

Like the previous cases the computational flow solver is ANSYS® Fluent v14, mesh has been imported and simulated with a two-dimensional steady-state flow domain, for a fully turbulent compressible ideal gas in double precision.
Using this solver condition the first step is to scale the mesh from meters to millimeters and fix the type solver on pressure-based.
Now the second step is to define the turbulence model:

- Energy on
- K-w SST

Fluid material:

- air
- density: ideal gas
- Cp: constant=1009.4[J/Kg*K]

Boundary Conditions at inlet:

- Pressure-far-field
- Static pressure: 100000[Pa]
- Mach number: 1.086
- X-component of flow direction: 0.52249
- Y-component of flow direction: 0.85264
- Turbulence method: Intensity and hydraulic diameter
- Turbulence intensity: 5%
- Hydraulic diameter: 0.04
- Temperature: 440[K]

Boundary conditions at outlet:

- Static pressure:130000[Pa] (for the first attempt to find UI conditions)
- Turbulent method: Intensity and viscosity ratio
- Backflow turbulent intensity: 5%
- Backflow turbulent viscosity ratio: 10

- Backflow total temperature: 544.26[K]

The solutions step-up has been changed during the simulation in order to better reach and support the convergence: the solution scheme has been fixed on coupled for all simulations and the gradient scheme on Green-Gauss Cell Based. The other derivative parameters (Pressure, Density, Momentum, Turbulent kinetic energy, Dissipation rate and Energy) have been fixed on first order in order to favor the successive convergence of second order. The solution controls have been fixed as now described:

- Flow courant number = 20
- Relaxation factor momentum = 0.4
- Relaxation factor pressure = 0.35

This only for the first 150 iterations to support the convergence, then for the others has been changed in:

- Flow courant number = 50
- Relaxation factor momentum = 0.5
- Relaxation factor pressure = 0.5

These options, both the lower courant number and relaxation factors, have been used also in the second order derivative iterations. The convergence has been established when all residuals go under 1e-05. Finally the flow has been initialized first with an hybrid initialization and then with fmg-initialization.

Because the test case have been realized at spill point condition, the solver options have been changed during the simulations by the Matlab code in order to find the UI conditions before and then the spill point pressure. So the flow angle during the UI loop and the static back pressure in the spill point loop have been changed in order to reach the respective conditions.

6.3 Results and validation

At the conclusion of each simulation, the parameters of interest have been calculated particularly with a *mass-weighted average* surface integral for static pressure at inlet and outlet surface and also for Mach number and velocity angle at inlet surface. Total pressure survey has been calculated with *area-weighted average* surface integral. Moreover the y+ parameter has been measured (and checked minor than 1) in order to confirm the goodness of the turbulence model.

The test case has been realized at spill point conditions, so when that pressure ratio is reached is possible to check the experimental test data with the numerical data. The figures below compare the pressure ratio p/pt_1 for the experimental and the numerical simulations:

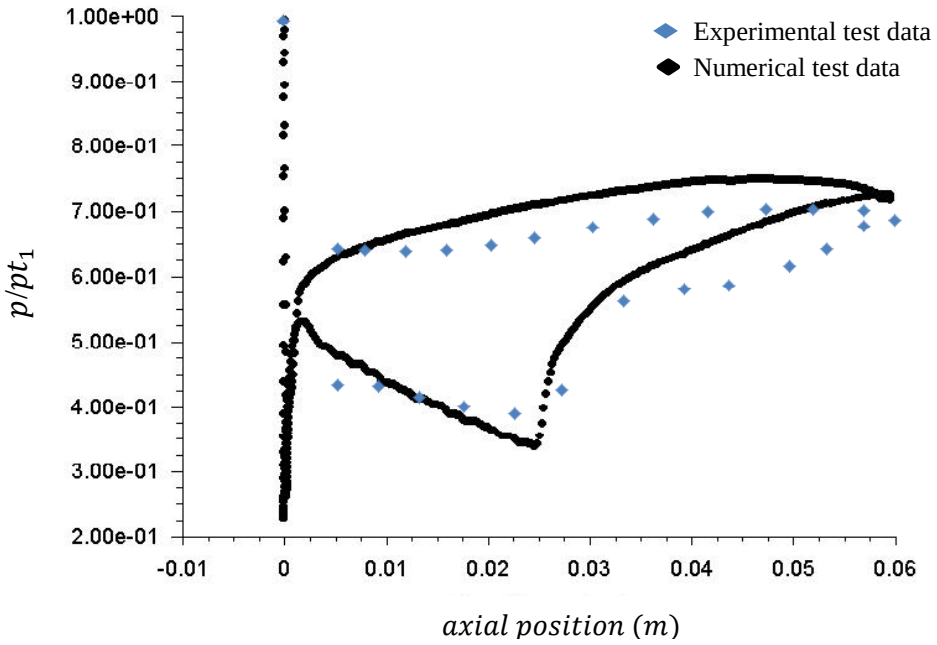

Figure 6.4 : Pressure values in function of axial chord position

First of all is important notice that the numerical spill point pressure ratio is p2/p1=1.583 instead of the experimental one that is 1.448. This important difference is due to the important AVDR difference between the two tests(as already seen in the Double Circular arc tests): AVDR=1 for numerical tests and AVDR=1.184 for experimental test, in fact an AVDR greater than 1 tends to move the shock upstream along the chord wise and so the spill point is reached for a lower pressure ratio.

Comparing the pressure diagram in the two cases: it is clear that the numerical points trace very well the experimental one, particularly the maximum isentropic Mach number just before the shock wave on the suction side, in the former zone of the blade and also in the rear zone and also on the pressure side. The only zone with a certain difference is just after the shock, where the numerical data have a greater slope, maybe also this is due to the difference in AVDR and this influence particularly a zone with a so complex flow and where the three-dimensionality of the flow is important. The same things appears comparing the isentropic Mach number[17] in the two situations, also here the numerical points trace very well the experimental one except for the zone immediately behind the passage shock. This graphic show a substantial agreement between the data obtained in the two situation, this agreement is also shown by the Mach number contour of simulation test and the experimental Schlieren picture:

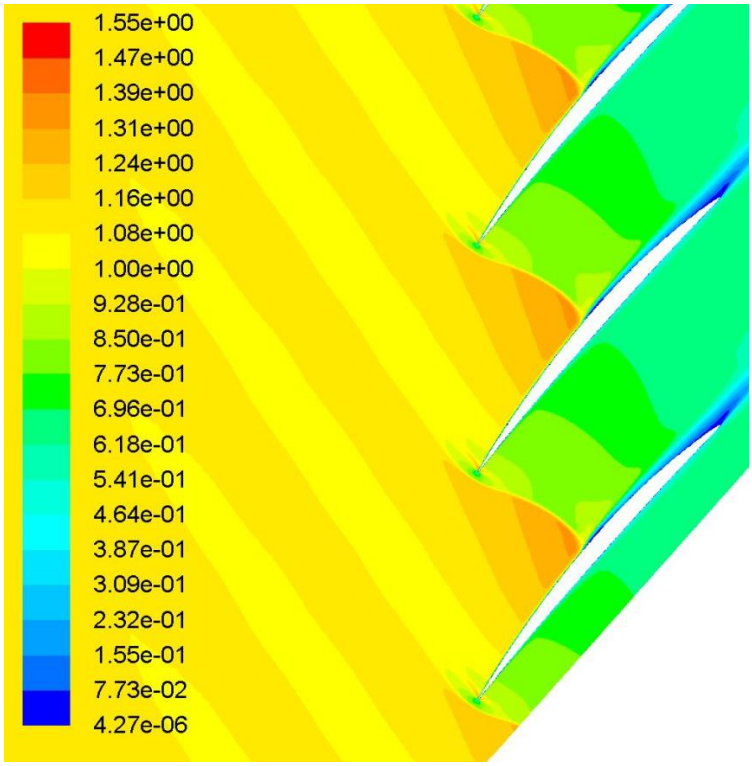

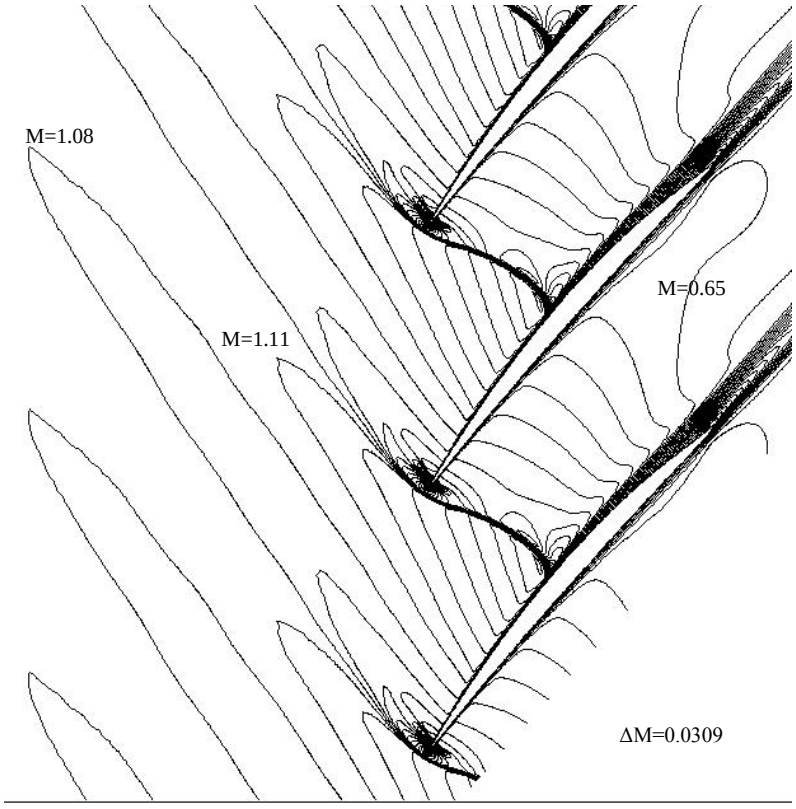

Figure 6.5: Mach number contours

Figure 6.6: Schlieren picture of experimental test[17]

The figures above shown a very good correspondence in the normal shock position and shape in the two cases and so the numerical simulation is validated also by the Schlieren test.

From figure(6.4) is possible to see that the flow is accelerated in the former zone by a series of expansion waves which deflect the flow towards the geometry of the blade. Maybe this is due also this time to the convex curvature of the inlet part of the blade. In the middle part of the chord wise there is a coalescence of the expansion waves in a quasi-normal shock, in fact the flow passes instantly from supersonic to subsonic and the flow field downstream the shock is completely subsonic, even if the shock shape is not perfectly normal. This shock is attached with the local normal shock wave that occurs at the leading edge of the successive blade. After the shock the interaction with the boundary-layer is very good with less separation of the flow despite the other previous two blades, this because the lambda shock in this case is strongly restricted. This is evident also calculating the loss coefficient that is very lower than the one of the previous blades:

$\omega=\frac{p_{01}-p_{02}}{p_{01}-p_1}$ =0.067

The reason of a lower lambda shock and so a greater efficiency of the blade can be explained in a more gradually acceleration of the flow due to the particular curvature of the former zone of the blade.

This shows the importance in controlling the former part of the blade, in this kind of blade the two circular arcs permit to have a better control on the shock waves at

the inlet region and so on the connected losses, proving that the first zone affects also the rest of the flow in the other blade parts.

7.S-shape blade

This kind of blades is the state of art of modern transonic axial compressors. Blades are composed by a particular S-shape suction-side, with a former concave zone at the suction side and a change in curvature at about the 60% of the chord. This particular concave surface at the leading edge guarantees a certain advantages that are shown below.

7.1Airfoil and cascade geometry

The airfoil geometry has been realized from the ARL SL 19 test case[18]. In this report the coordinates of the profile have been given a part for the leading and trailing edge that have been reconstructed in order to preserve the slope and curvature of the original profile. The blade and test characteristics are presented below:

- Chord length = 85 mm
- Stagger angle = 146.93°
- Pitch chord ratio = 0.654
- Inlet Mach number = 1.59
- Inlet flow angle = 147.9°
- Re = 1.12*10E06

Mass averaged exit

- Outlet Mach number =0.9355
- Outlet flow angle = 147.9°
- Pt2/pt1 = 0.9116
- AVDR = 1.128
- ω = 0.1161
- p2/p1 = 2.175

Contrary to the previous tests case, this test case has not been simulated at spill point but at a particular pressure ratio with a lower static back pressure, so the wave pattern is confined in the blade passage. The particular pressure ratio that realizes the same condition of the experimental test is higher because of the presence of AVDR, however the conditions of the test are of UI and so has been realized the Matlab loop to find these conditions. The inlet flow angle measured is a little bit different from the experimental one because the leading edge does not trace perfectly the original profile.
The figure below shows a scheme of the cascade geometry with all its parameters:

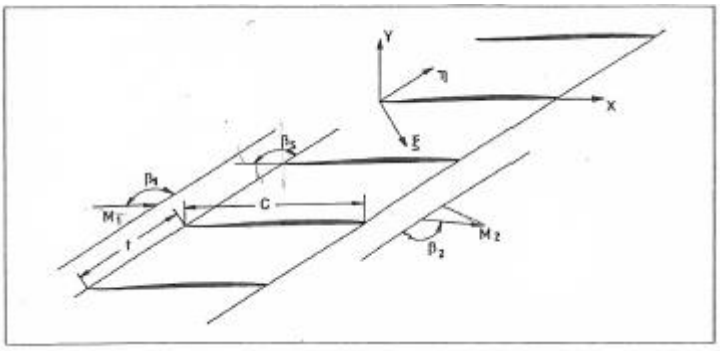

Figure 7.1: S-shape blade design[18]

7.2Flow solver and computational domain

The flow domain has been solved by the use of a structured mesh realized with ANSYS® ICEM. This software is very powerful and flexible in fact the same blocking structure of the MCA blade can be used to create the new mesh with few adjustment. Hence also this time the inlet face has been fixed at 1,5*chord length and the outlet face at 2*chord length. The nodes have been located increasing their number in the former zone, leading edge and trailing edge, the general number is quite similar to the previous one because the dimension of the two blades are comparable.

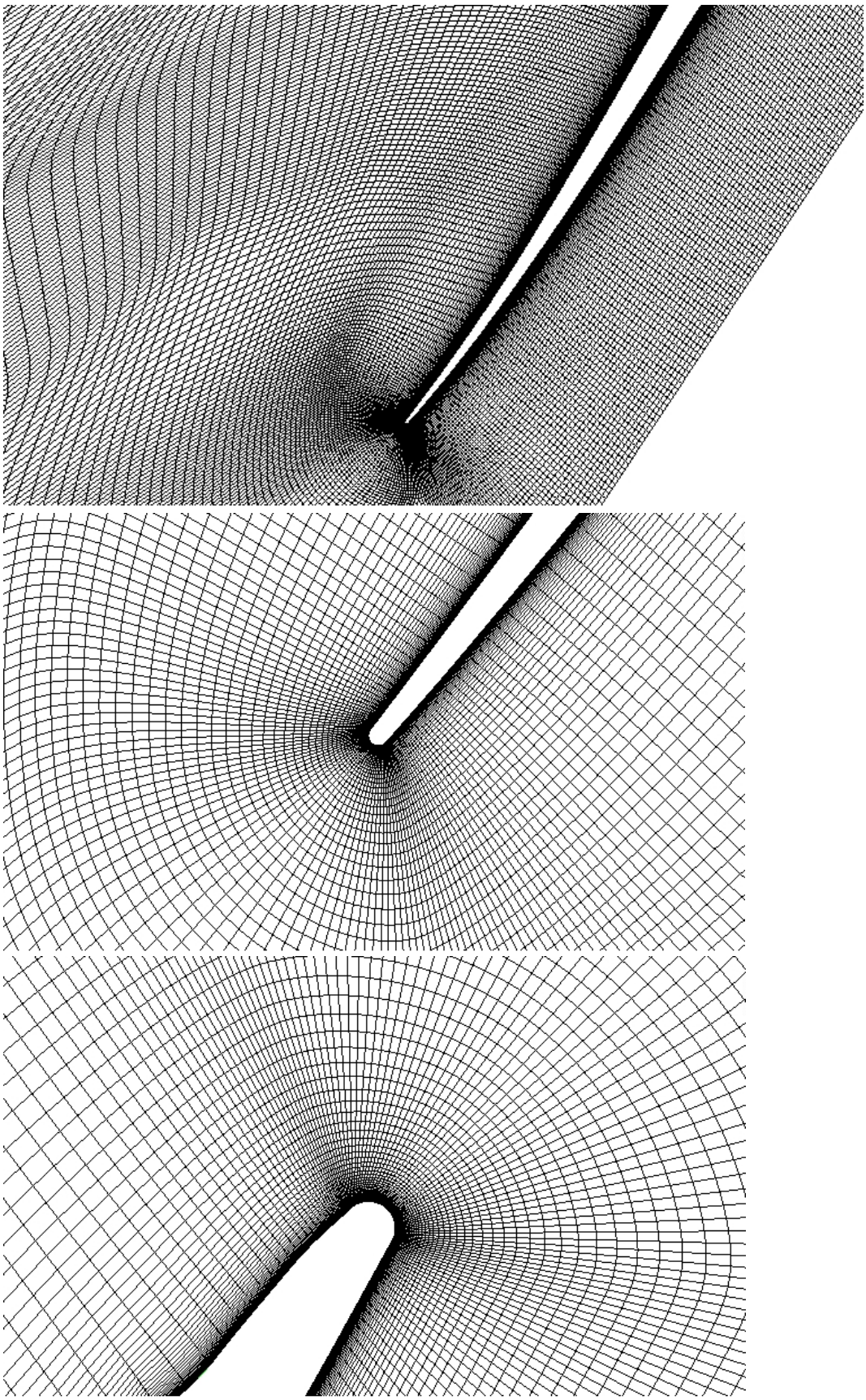

Figure 7.2: Mesh structure front zone (first), LE (second), TE (third)

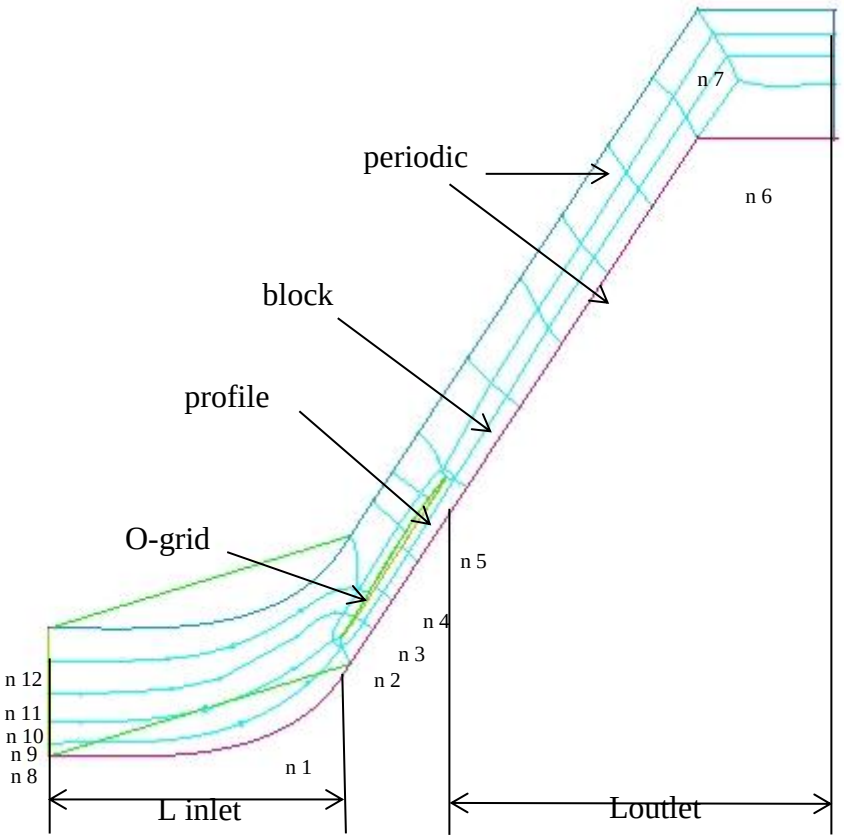

Figure 7.3: Blocking structure of S-shape blade

Variable description	Variable	Nodes
Inlet	n 1	85
PS front zone	n 2	74
PS middle1	n 3	50
PS middle2	n 4	65
PS rear zone	n 5	125
Outlet	n 6	35
Trailing edge	n 7	50
Inlet lower zone	n 8	26
Leading edge	n 9	35
SS front zone	n 10	60
SS middle	n 11	45
Inlet upper zone	n 12	39
O-grid layers		67
O-grid growth rate		1.07
O-grid first layer		0.0004

The table above shows that substantially the blocking distribution and the nodes number remains constant; this explain how powerful is this mesh tool particularly

with these profiles that have a similar shape and so the blocking structure can be preserved in the various simulations.
Realized the structure, the successive step is to realize the unstructured mesh and smooth this with the following parameters:

- Number of iteration on surface: 10
- Smooth type on surface: Laplace
- Freeze options: selected parts
- Smooth along curves: None

The mesh quality has been checked with the same parameters of the previous blades: *quality, aspect ratio, skew.* The definition of these parameters is the same discussed in 4.2, the value for this type of mesh is reported in the table below:

Grid quality	min	max
Quality	0.5	1
Aspect ratio	0.001	1
skew	0.16	1

All the parameters are substantially good in accordance with the other, and this can be expected because the mesh has the same characteristic of the previous.

The mesh is now ready to be analyzed by the computational solver ANSYS® Fluent v14, the conditions in which this software works are two-dimensional steady-state flow domain, for a fully turbulent compressible ideal gas in double precision.
The first step is to scale the mesh from meters to millimeters and fix the type solver on pressure-based.
Now the successive step is to define the turbulence model:

- Energy on
- K-w SST

Fluid material:

- air
- density: ideal gas
- Cp: constant=1009.4[J/Kg*K]

Boundary Conditions at inlet:

- Pressure-far-field
- Static pressure: 100000 [Pa]
- Mach number: 1.59
- X-component of flow direction: 0.5314
- Y-component of flow direction: 0.8471
- Turbulence method: Intensity and hydraulic diameter
- Turbulence intensity: 5%
- Hydraulic diameter: 0.04

- Temperature: 361[K]

Boundary conditions at outlet:

- Static pressure:230000[Pa] (for the first attempt to find UI conditions)
- Turbulent method: Intensity and viscosity ratio
- Backflow turbulent intensity: 5%
- Backflow turbulent viscosity ratio: 10
- Backflow total temperature: 544.26[K]

The solution options have been changed during the simulation in order to favor the convergence and simplify the second order convergence; for all the iterations the solution scheme has been fixed on coupled, and the gradient scheme on Green-Gauss Cell Based. The derivatives solution(Pressure, Density, Momentum, Turbulent kinetic energy, Dissipation rate and Energy) have been fixed on first order in a first step, and then after their convergence have been turned in second order. The solution controls have been imposed as shown below:

- Flow courant number = 20
- Relaxation factor momentum = 0.4
- Relaxation factor pressure = 0.35

This only for the first 150 iterations to support the convergence, then for the others has been changed in:

- Flow courant number = 50
- Relaxation factor momentum = 0.5
- Relaxation factor pressure = 0.5

This process has been repeated also for the second order derivative. The convergence has been established when all residuals go under 1e-05 and the flow has been initialized first with an hybrid initialization and then with fmg-initialization. In the boundary inlet conditions the X-component of flow direction and Y-component of flow direction have been changed during the simulations in order to reach the UI inlet flow angle by the use of a Matlab code. Despite the other blades in this case it has not been reached the spill point back pressure because the experimental test has been conducted in other backflow condition.

7.3 Results and validation

The numerical solver outputs have been calculated in the following way: *mass-weighted average* surface integral for static pressure at inlet and outlet surface and also for Mach number and velocity angle at inlet surface; total pressure survey has been calculated with *area-weighted average* surface integral. Also in these simulations the y+ parameter has been kept under 1 in order to confirm the turbulence model.

The test case has been simulated at a lower back pressure than the spill point and this is evident from the Schlieren picture (Figure(7.5)) , so initially the back

pressure that match the test conditions has been found. Hence with the Matlab code the UI conditions for that pressure ratio have been reached.

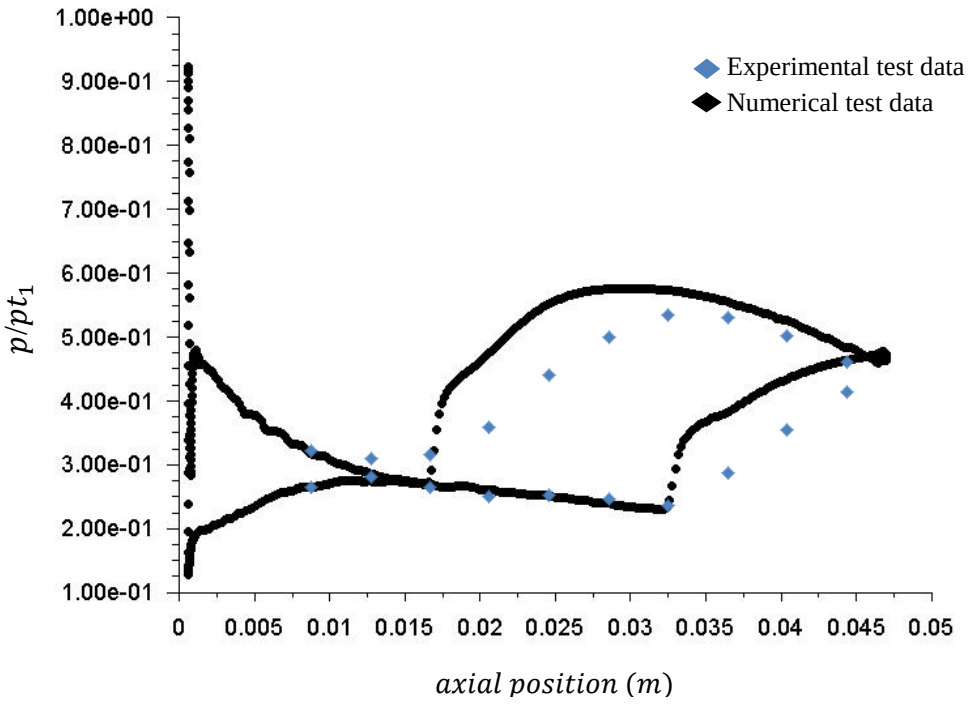

Figure 7.4: Pressure value in function of axial chord position

Initially it is worth notice that the numerical simulations have been conducted at a greater static pressure ratio than the one reported in experimental test. This can be explained with the difference in AVDR between the two cases: AVDR in experimental test is 1.117 instead in numerical simulation AVDR is 1. As already said, a greater value of AVDR tends to move the shock wave upstream and so the wave reach the condition exposed in the diagrams for a lower pressure ratio than that case when an AVDR is unitary.

The figure shows that the numerical points trace very well the experimental one, and also in the diagram of isentropic Mach number the maximum isentropic Mach number in correspondence of the wave is traced very well. Like the MCA diagrams, the only zone where the two points series shows a discrepancy is just after the shock and this is clear also seeing the isentropic Mach number [diagram[18]] where the simulated points shows a greater value than the experimental. This behavior can be explained by a three-dimensional loss that can occur in the experimental test because of an AVDR difference from one that the numerical solver can‘t capture.

The numerical flow field can be checked also with the Schlieren picture, which shows the wave position and pattern. Even if the picture is not so clear, however is evident the correspondence of the oblique shock in the two cases:

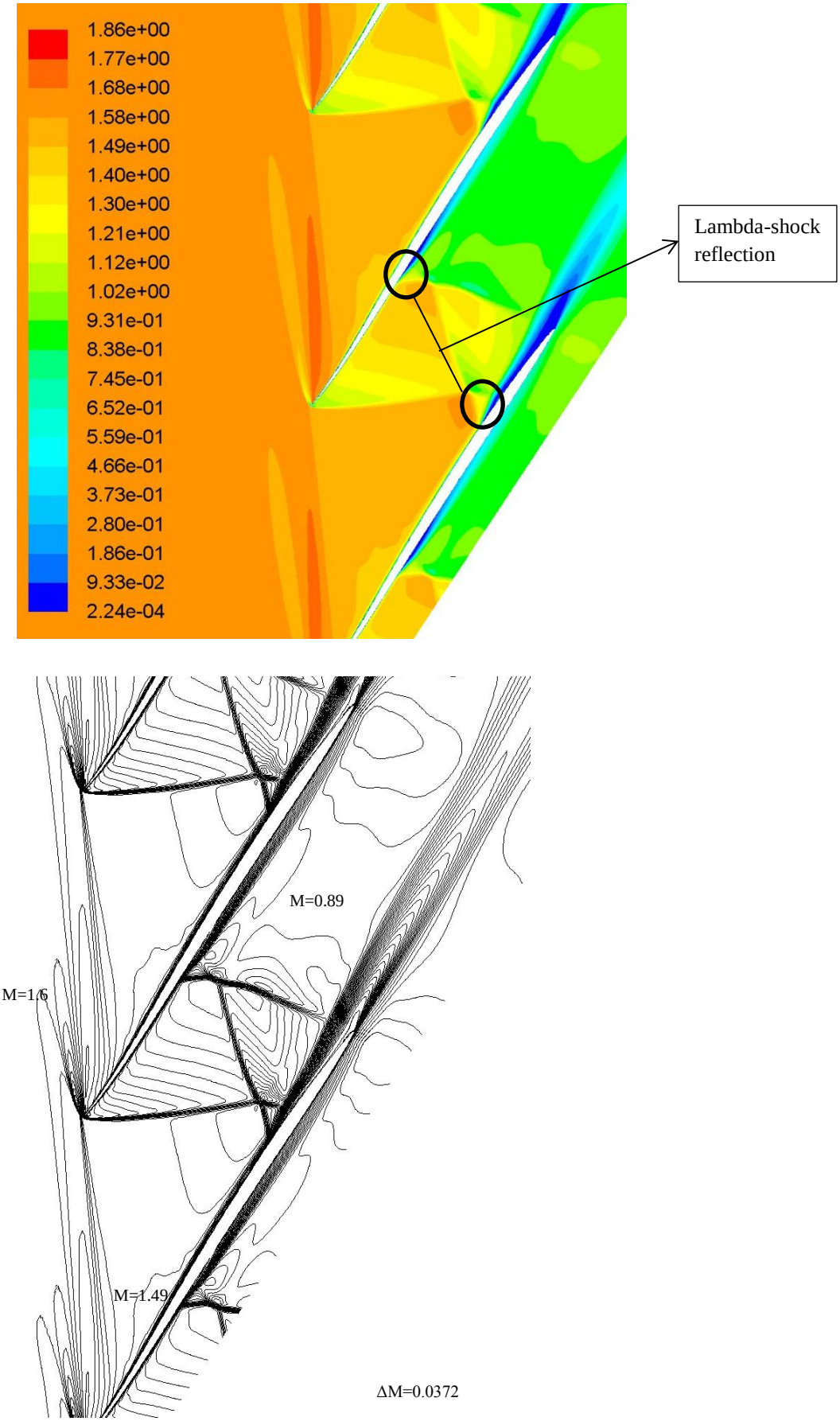

Figure 7.5: Mach number contours

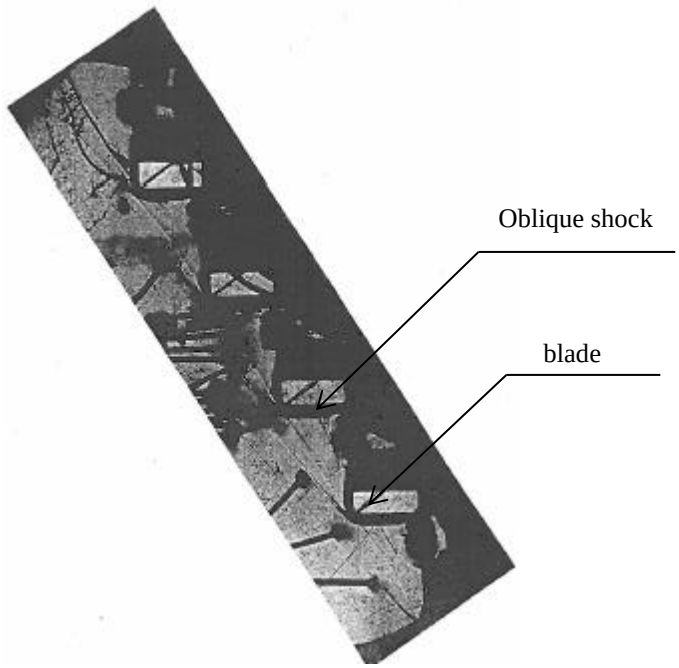

Figure 7.6: Schlieren picture of experimental test[18]

As the two figures show, the oblique shock has the same shape in both numerical and experimental test. Figure (7.4) shows the particular flow field that occurs in the blade passage: at the leading edge of the blade the flow encounters a series of expansion waves that accelerate the flow and deflect it towards the blade shape. Hence a series of pre-compression waves decelerate the flow slightly till it encounters the strong oblique passage wave, which decelerates the flow further. Immediately below such oblique shock, there is a quasi-normal shock whose interaction with the boundary-layer gives rise to the lambda shock system. Behind the normal shock the flow passes instantly from supersonic to subsonic. Similarly behind the lambda shock the flow is subsonic, even if in the lambda shock the flow is decelerated more gradually. Behind the oblique shock passage the flow experiences a new acceleration : this because of a series of expansion waves, then a new oblique shock decelerates definitively the flow to subsonic. This new oblique shock is the result of reflection of previous oblique shock in fact it is possible to see a little new lambda-shock on the pressure side of the following blade, so there is also a lambda shock reflection.

At the rear zone of the blade occurs always a certain separation of the flow but it is important consider that the pressure ratio is not the spill point's one (more efficiency is present at spill point condition) so despite the other blades this does not work at maximum of efficiency. However the loss coefficient assumes an acceptable value, also comparing it with the previous blade:

$\omega=\frac{p_{01}-p_{02}}{p_{01}-p_1}$ =0.126

In conclusion, the concave curvature at the former zone of the blade assumes a dominant role; in fact this shape of the blade permits to convert the normal shock in the passage in an oblique shock. This conversion is the key to understand the improvement in loss coefficient as the normal shock is more dissipative than the oblique one. Therefore the deceleration of the inlet flow by pre-compression waves and the oblique passage shock contribute to reduce the loss and increase efficiency.

In uniformity with the other blades, also for this typology the spill point simulation has been realized:

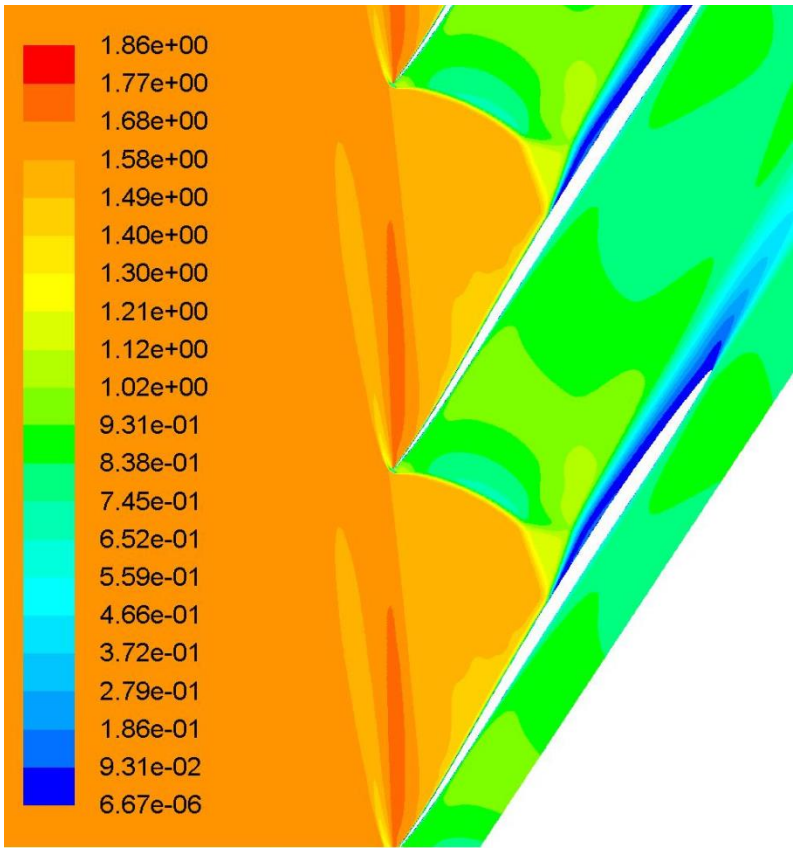

Figure 7.7: Mach number contours at spill point condition

Also from this figure is clear that the separation that occurs at the rear of the blade is limited, and also the lambda-shock is very little thanks to the pre-compression waves that reduce the strength of the passage shock wave.

8.Blade Comparison

All the previous analysis shows the importance of blade profile in the flow upstream the shock, in the shock pattern and strength and on the separation of the flow in the rear part. So to better analyze the behavior of the flow in function of the blade shape evolution here are compared the blades all together:

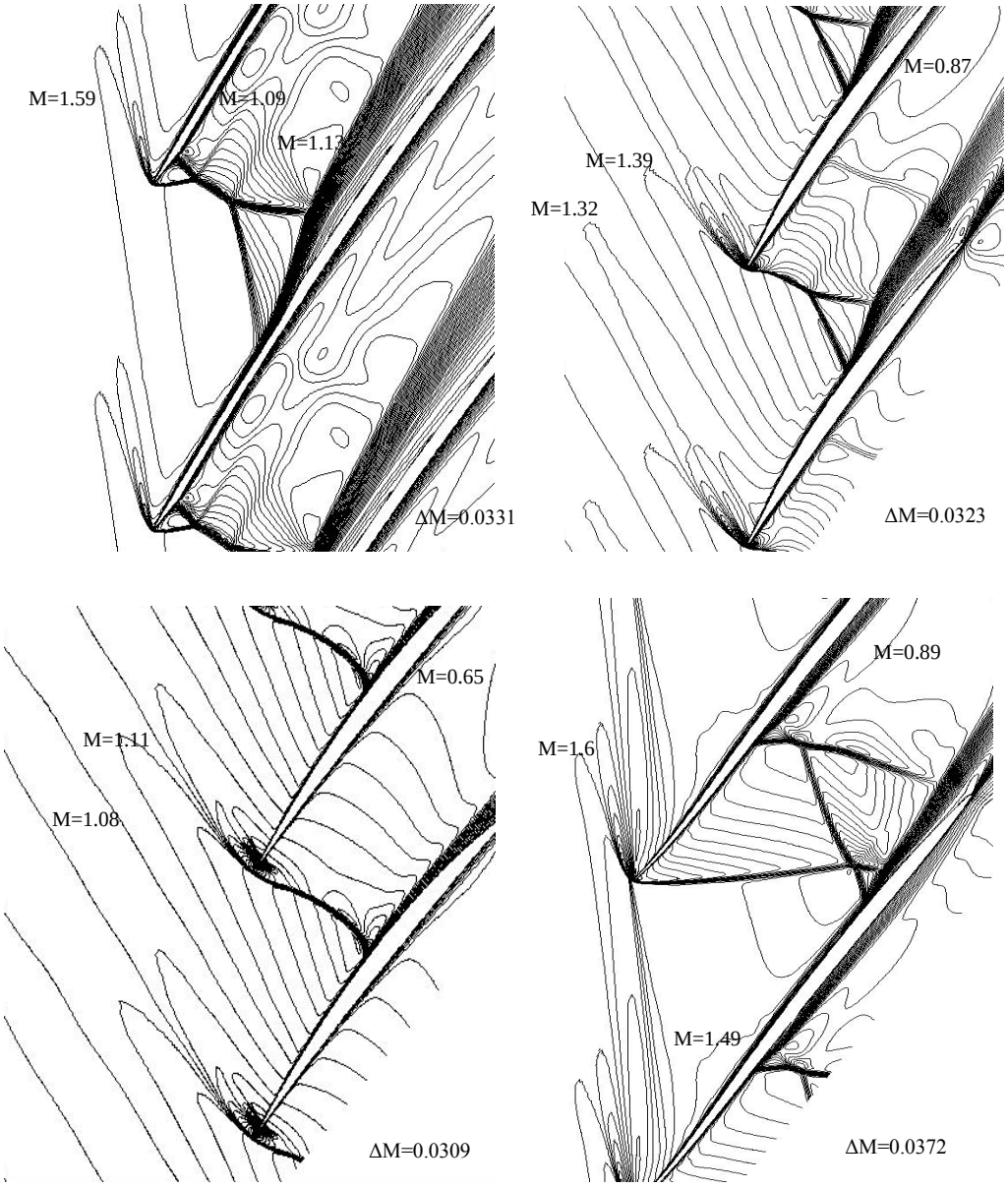

Figure 8.1: different shock pattern for the blades, starting from the high left in clockwise: Kantrowitz, DCA, S-shape.MCA.

From the observation of all the blades' flow field, is clear that all of them show an initial series of expansion waves at the former region that adapts the flow to the blade. This happens in all the blades with waves starting from the leading edge and spreading upstream. What discriminate the various blades is how the flow adapts itself to the blade shape after this first expansion wave: Kantrowitz blade accelerates the flow with a strong expansion wave, the DCA blade accelerates the flow with series of expansion waves which accelerate the flow progressively towards the normal shock. Also the MCA blade accelerates the flow but in a different way that is more gradually than the DCA and in a way that the wave front is more regular. It is important notice that all these blades approach the shock with expansion waves but the shock pattern is strongly different each other, certainly this can be attributed to 1) the shape of the former part of the blade and 2) the axial position of the maximum thickness on the blade. In fact observing the first two blades and particularly comparing them with the MCA blade is possible to see that the first blade accelerates immediately the flow to high Mach number for the entire blade passage and so the blade lambda shock is extremely developed; instead the DCA blade accelerates the flow more gradually with three different Mach-number for the expansion waves, this makes the shock less strong than the precedent and so the lambda shock is not so extended like the previous blade (in both case the strength of the shock forms a quasi-normal shock, whose interaction with the boundary-layer gives rise to the lambda shock).

Considering now the MCA blade, this has a little lambda shock and the expansion waves increase velocity step by step without great zone of high velocity. Hence a little by little increase in velocity doesn't provoke great losses and this is highlighted by the loss coefficient that is very small in the case of MCA blade. So it is worth notice that high velocity in blade passage is the main reason of great lambda shock and consequently of great losses.

The differences in the geometry of this three blades lead to understand that the more the maximum thickness is near the leading edge the more the expansion wave is strong and the flow accelerated is dissipative, this is clear comparing mainly the first two blades. Moreover considering the particular shape of the MCA blade is possible understand also that the more the former zone is convex the more the flow is accelerated and the strength of the passage normal shock increase, giving rise to great lambda shock and losses. In fact in the MCA blade the lambda shock is very little and the expansion waves accelerate gradually the flow, hence the coefficient loss is strongly lower than the other two.

The size of the lambda shock affects also the importance of flow separation at the rear part of the blade and the losses connected: a great lambda shock implies a great separation of the flow and so great entity of the losses.

What has been said above is about the blades which operates with expansion waves in the former part, but s-shape operates with pre-compression waves. The pre-compression waves contribute to compress the flow, moreover in this kind of blade the presence of oblique passage shock instead of quasi-normal shock

converting the flow from supersonic to subsonic, contributes to reduce the losses (oblique shock is less dissipative than normal).
The reason of these pre-compression waves is in the concave former zone of the blade, this permits to develop this kind of wave very useful to decelerate the flow and favor the successive compression with little loss, also the lambda shock is limited and consequently the connected losses. To this result contributes also the position of maximum thickness that is located at about 60% of chord, so particularly downstream on the blade.
In conclusion comparing all the blades what can be said is that the former zone till the maximum thickness is the most important zone of all the blade, in fact the strength and the typology of the shock wave are affected by the shape of this part. Particularly is important to have the maximum thickness position over the middle of the blade chord and the shape of the former zone must have a little convex or better a concave curvature respectively to limit the acceleration of the flow or to compress it. The case of concave curvature is to prefer because the pre-compression wave decelerates the flow and the successive shock is an oblique shock instead a normal sock which is more efficient. At the end of this chapter is important observe that an increase in efficiency could be obtained theoretically reducing the leading edge thickness, in fact from theory of oblique shock this implies a reduction of shock angle that means a reduction in shock losses. Practically this solution is not feasible because a too thin leading edge gives rise to structural and manufacturing problems.
In the parametrization that will be explained below the considerations on the importance of the former zone of the leading edge leads to define with the Bèzier curve only this first zone fixing the rest of the blade.

9.Geometrical parametrization

When a shape optimization has to be made, is important to realize a good parametrization of the profile , in fact to manipulate directly the blade coordinates requires a prohibitive computational cost because of an excessive number of decision variable. Hence the parametrization permits to reduce the DOF being able to describe however the geometry. So the characteristics of a good parametrization are:

- A low number of variable to describe the considered geometry
- Enough degrees of freedom to allow the optimization algorithm to explore all the feasible solutions.

It is clear that these two aims go in different direction in the choice of the number of decision variables. In fact a great number of DOF leads to a huge research space for the possible shape but requires a high computational power and time resources. On the other hand a lower number of variable is easier to compute but reduce research space to find the optimal shape. The classical parametrization methodologies are Bèzier curve or cubic spline. In this thesis Bèzier curve method has been used and so this type of curve is described below.

9.1 Bèzier Curve

Every curve can be represented by its Bèzier polygon, in fact the Bèzier curve is the result of the Bèzier polygon and have the characteristic that the curve has the same end points and tangents, and the curve lies in the convex part of the polygon. Bèzier curves are parametric with t included between 0 and 1, the curve is represented by the expression:

$$\begin{Bmatrix} x(t) \\ y(t) \end{Bmatrix} = \Sigma_{i=0}^{n} C_{n,i} * t^{i} * (1-t)^{n-1} * \begin{Bmatrix} x(i) \\ y(i) \end{Bmatrix} \qquad t \in [0,1]$$

$$C_{n,i} = \frac{n!}{i! * (n-i)!}$$

In the expression above x(i) and y(i) are the coordinates of the control points of Bèzier polygon. The characteristics of the curve are:

- Joining the point of the Bèzier polygon with lines, the curve is tangent at the first and ta the last segment
- The curve has a degree equal to the control points-1
- The curve does not cross any point except the first and the last.

It is worth notice that are several the way of realizing a parametrization, each time is important to find the adapt variable which better describe the shape, without exceed in the number in order to reduce the computational cost.

9.2 Profile parametrization

From the observations conducted in chapter 8 is clear that the most important role in a transonic blade is played by the former zone of the suction side, mainly from its shape and the position of maximum thickness. Hence has been decided to realize the parametrization of this first part maintaining fix in the original shape the rest of the blade. In figure(9.1) is highlighted in blue the zone described with Bèzier curve and in red the fix zone.

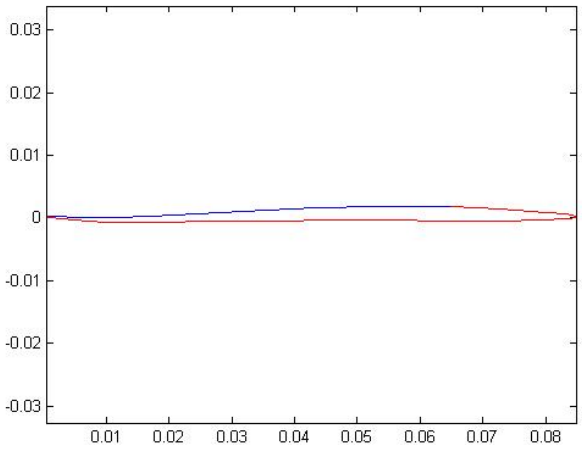

Figure 9.1: Parametrized profile in blue and fixed profile in red

In this way is possible to understand how strongly this part influences the performance of the cascade, so how is important to concentrate the attention on this zone modifying only this region and observing the consequently changing in performance that this provoke.
To preserve the continuity of the profile has been imposed the constancy of the first and second derivative for the initial and the last zone of the modified part with the derivatives of the fixed part. Moreover is important notice that the leading edge radius has not been changed during the optimization(so it does not belong to the parametric region). So considering this limitation the number of variable of decision has been decided to be in number of six: 1) x-coordinate for the first point of Bèzier polygon, 2) x-coordinate for the second point of Bèzier polygon, 3) x-coordinate for the third point of Bèzier polygon,4) y-coordinate for the third point of Bèzier polygon,5) x-coordinate for fourth point of Bèzier polygon, 6) x-coordinate for the fifth point of Bèzier polygon. The y-coordinates of the first, second, fourth and fifth points are fixed by the condition of constancy of the first two derivatives at the beginning and at the end of the curve. This device is useful to create always a profile acceptable and without discontinuities.
This parametrization permits to evaluate huge shape of the blade and so to understand the role that this part play in increasing the performance.

10 Genetic algorithm

Generally an engineering optimization problem consists to improve the performance of existing design. For example in a turbine could be interesting to find the shape which reduce the loss coefficient, and increase the work of the turbine. Depending on the number of objective the problems could be mono-objective or multi-objective, the mono-objective involves the maximization or minimization of a single objective, instead a multi-objective involves the maximization or minimization of two or more objective. The optimization algorithms can be divided in deterministic and stochastic, there are several optimization methods: Random search, random walk, simulated annealing, evolutionary algorithms, first order methods and second order methods, Newton method. In this thesis work has been used a genetic evolutionary algorithm so now some characteristics of this method will be exposed:

- This method calculates absolute global maximum and minimum (not local)
- Works with operators based on deterministic and stochastic logic, so it ia s pseudo-stochastic method
- Doesn't need the evaluation of partial derivative
- Works with a population of possible solutions and not a single one.

This algorithm is based on the evolution natural process, that means an evolution from generation to generation in a way to increase the better elements in the population. The algorithm starts with an initial population, every single individual is joined in bijective way with his chromosome and each chromosome is identified by a binary string containing all values of parameters. The genetic material is manipulated and then the best elements are chosen to realize reproduction and so create a population of sons. Hence the elements which best adapt themselves to the environment have greater possibilities of transmitting the genetic makeup. In this way proceeding with generations the medium fitness increases. This genetic evolution is repeated for the chosen number of generation.
To represent every element with binary representation is necessary to pass from real numeration to binary , hence a value x (x^l<x<x^u) can be represented in binary sting S=[b_q, b_{q-1},… b_2, b_1, b_0]; so the value x can be rounded by the binary string with :

$$x = x^l + \frac{\Sigma_{k=0}^{q} bit_k * 2^k}{2^{q+1}-1} * (x^u - x^l)$$

where q is the number of bit, the greater is the number of bit, greater is the definition of x; and bit can assume the value 0 or 1. If n is the number of variable of decision and the number of element in the binary string is q+1:

$x_1 = \begin{Bmatrix} string(1) \\ . \\ . \\ . \\ string(n) \end{Bmatrix}$ n rows, q+1 columns

If all the columns are shifted on only one row and this operation is repeated for all the elements, the result is a matrix containing all the chromosomes of the variable.

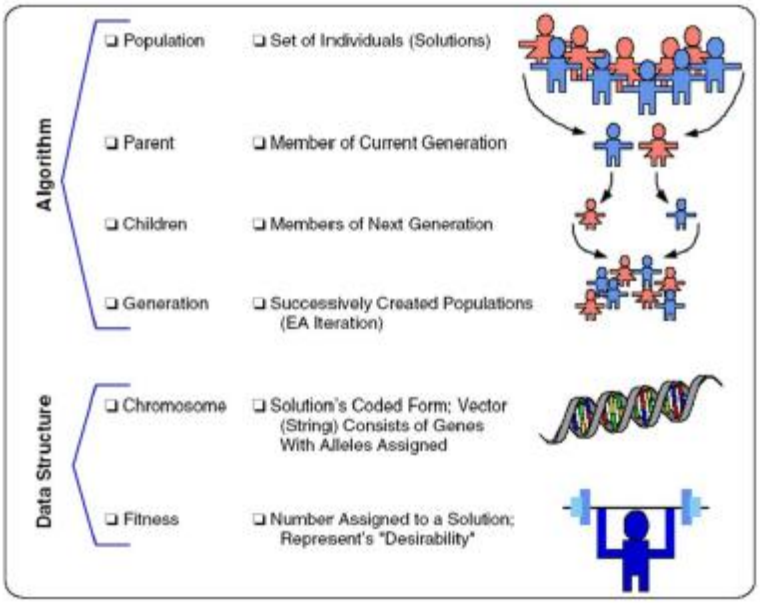

Figure 10.1: GA reproduction mechanism

The only criterion between the variable of decision is the fitness function f(X).

10.1 Genetic algorithm operators

In order to guarantee the correct evolution of generations and to explore the widest research space three GA operators are used:

- Selection
- Reproduction
- Mutation

These must be used in this order to guarantee the correct evolution.

Selection

The selection operation can be realized in two different ways: *tournament selection* and *roulette wheel selection.* In the first method the algorithm chooses

randomly two elements of the population and compares the fitness value for example if f(x_i)<f(x_j) (problem of minimum) the xi element is chosen. So in the operation of choice of the elements stays the stochasticity, while in the comparison of the fitness stays the deterministic operation.
In the second method all the individuals are represented in a circle which is divided in some parts one for each individual proportionally to the fit. Turning the roulette with a random counter is chosen the specific individual. Hence in the division of the circle stays the deterministic operation(larger space in the circle means greater probability of choice), while in the random choice the stochastic operation.

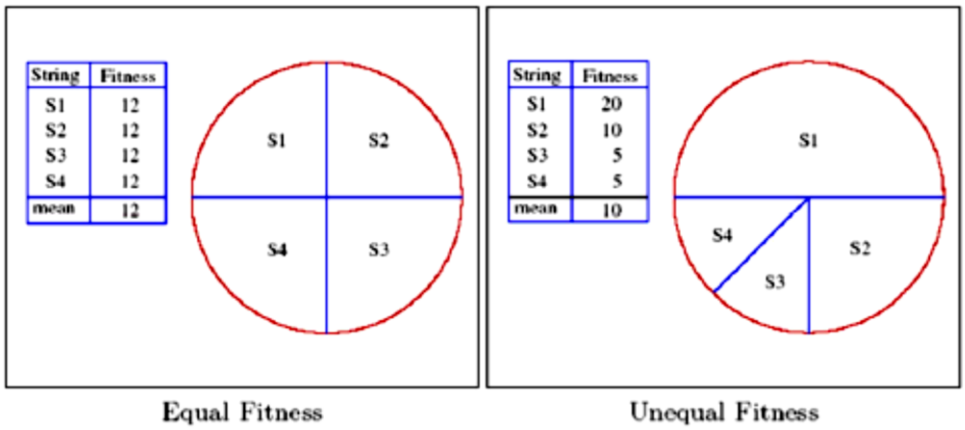

Figure 10.2: Roulette selection mechanism

Reproduction

This operation allow to create the individuals child from the parents. In the chromosome of the parents a random counter the *crossover* that divides the two chromosome (binary string); hence the two parts are exchanged obtaining the two sons. The crossover random counter realizes the stochastic operation, while the exchange in chromosome parts realizes the deterministic one. It is possible also to have two or more crossover counters that break the chromosome in more points(increasing stochasticity). Generally the reproduction operation generates a population of sons with better fitness value.

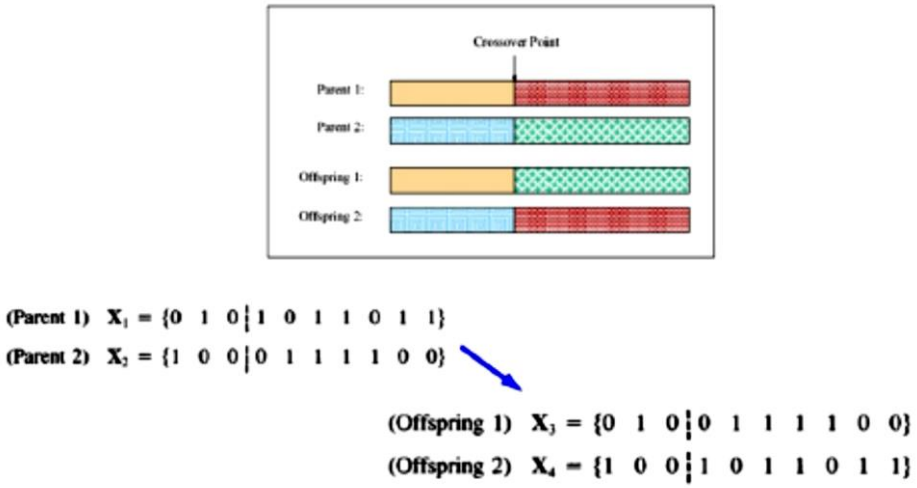

Figure 10.3: **Crossover mechanism**

Mutation

In a some percentage of the child population the algorithm changes casually a 0 element in 1 or vice-versa, the aim of this operation is to free the child population from the parent's one, moreover helps the algorithm to find the real Pareto front. Most genetic algorithms use elitism strategy in order to preserve the best individuals from the operation of mutation.

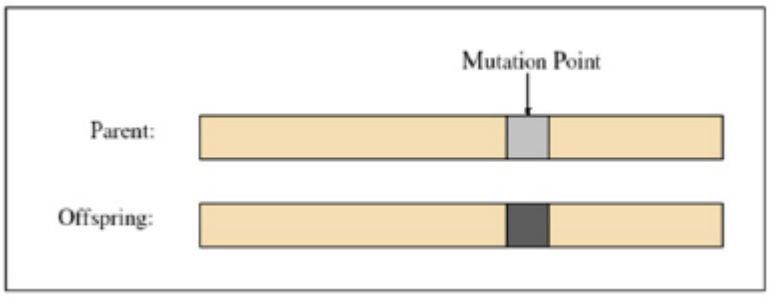

Figure 10.4: **Mutation mechanism**

10.2 Methods of genetic diversity preservation

When the algorithm proceeds in the generations the optimization, it cold move towards an incomplete Pareto front because of an insufficient domain exploration. To avoid this risk, two methods of preserving the genetic diversity can be used: *fitness sharing* and *crowding.* In the first method for every solution on the front a circular zone is defined with an arbitrary radius (it is reduced during the optimization), hence the elements contained in the circular zone more dense of

individuals are penalized with a function of penalization. The second method is quite similar: considering a particular point, a rectangular zone is created using the point before and the point after. The zones more dense in elements will be penalized , the advantage of this method is that there isn't any arbitrary parameter, the disadvantage is that is penalized the zone near the more dense zone.

10.3 Pareto ranking

In multi-objective problem, find the best solutions of the problem is not banal, in fact is impossible to maximize together f(x1) and f(x2), the best way is to create a Pareto front in which a group of solution is better than all the others. The Pareto front is based on the concept of dominance; a solution dominates another when are satisfied the following two conditions:

- Solution x^1 is not worse than x^2 for all the objective functions: $f_j(x^1) < f_j(x^2)$ (for min.) or $f_j(x^1) > f_j(x^2)$(for max) for all j=1…n
- Solution x^1 is strictly better than x^2 at least in one objective function: $f_j(x^1) < f_j(x^2)$ (for min.) or $f_j(x^1) > f_j(x^2)$(for max) at least one j=1…n

If this two conditions are verified solution x^1 dominates solution x^2.

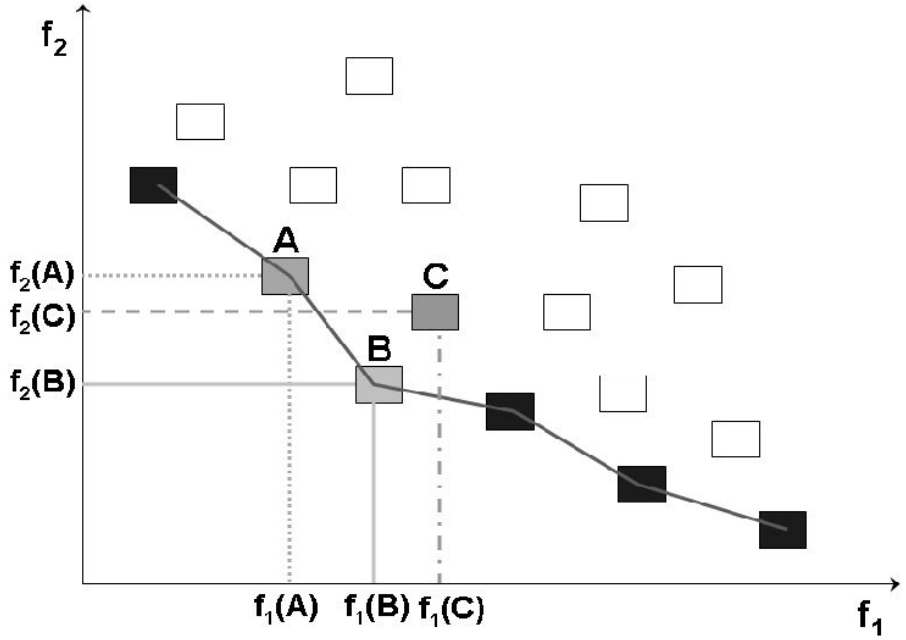

Figure 10.5: Pareto ranking diagram

Figure(10.5) shows a Pareto front, solutions A and B belong to the front, while C is a dominated solution; in fact considering solution B and C, B is not worse than C in both f_1 and f_2, moreover B is strictly better than C in both f_1 and f_2. So C is dominated by B, considering solution A and B, is clear that none of them

dominates the other so they belong to the Pareto front, in fact the Pareto front contains all the non-dominate solutions.

11. Optimization strategy

In this chapter will be exposed how the optimization routine has been set up, hence the number of decision variable, the parametrization used for the profile, all the options used in the algorithm and the results obtained.

11.1 Profile parametrization

As already said in 9.2, the profile has been parametrized only in the former zone of the suction side in order to understand the importance of this part in blade performance. The profile has been parametrized with Bèzier curve to control the surface deformation, and the first and second order derivatives of the two extremities of the curve (to preserve the continuity). The parametrized zone starts just after the leading edge zone till the zone just after the maximum thickness, the leading edge has been preserved because otherwise the algorithm tends to reduce the thickness till too thin value impossible to obtain from a manufactural point of view, in fact more thin thickness involves more efficient compression waves. Hence the number of points of Bèzier polygon are six and are that listed in 9.2 and so also the number of DOF are six. This number seems to be the better compromise between a good description of the profile and the computational cost that this number involves (in fact the number of individuals in the algorithm is proportional to the DOF).
The first profile for the initial population is the one simulated in chapter 7, so initially the baseline profile has been reconstructed in the zone parametrized with Bèzier curve using Matlab algorithm.

11.2 Algorithm set-up

The genetic algorithm used in this thesis is the one implemented in Matlab and so the genetic operators (selection, reproduction and mutation) used are the default Matlab operators. The most important parameters in genetic algorithm are: *number of individuals* and *number of generation.* A huge number of individuals is to prefer in order to evaluate completely the variable space, moreover a great number of generations allows the algorithm to find the optimal Pareto ranking and so the more interesting region from an optimization point of view. But it is also important to find a trade-off between the quality of results and the computational cost. So herein has been decided to operate with 7 individuals for each generation and with 3 generation, this even if is not a sufficient number to realize a complete optimization, is however sufficient to realize a first optimization and mainly can be useful to evaluate the improvement that can be obtained modifying this limited

zone. So it can be considered only a first qualitative step in which is important understand the magnitude of the variation in performance of the blade.
Moreover have been fixed the upper and lower boundaries of the algorithm in order to found the individuals of the new populations. About the initial population this is the result of a precedent work in which the variable of decision have been changed randomly in order to find acceptable geometries and so drive the algorithm towards shapes not too strange.
The aim of the multi-object optimization problem was to minimize the cascade loss and the inlet flow angle (this to maximize the mass-flow rate that the blade can elaborate):
F(P)=(f_1, f_2)=(ω,β_1)
Where P is the vector of decision variables, so the aim of optimization is to find the values of decision variables that minimize this two functions.
In order to find the correct value of inlet flow angle and to fix a common simulation condition all the profile has been simulated at unique incidence conditions, so for every profile has been conducted the UI control loop to find that conditions.
To reach these conditions for every individual has been constructed a ICEM mesh like already said in chapter 7.2, using journal file with the same characteristics used for the baseline profile. Again each profile has been simulated with ANSYS® Fluent v14, fixing the inlet conditions of the s-shape profile simulated in chapter 7:

- Mach number: 1.59
- X-component of flow direction: 0.5314
- Y-component of flow direction: 0.8471

And all the other inlet and outlet (outlet pressure 230000[Pa]) conditions listed in 7.2 also for the solution controls.

11.3 Discussion of results

At the end of the optimization process has been obtained a Pareto front of all non-dominated solutions, this front is plotted in Figure(11.1), where in blue are represented the non-dominated individuals while in red all the others. The baseline profile is identified with number zero, the elements which belong to Pareto front are identified with numbers one and two. The first element belongs to the initial population, while the second belongs to generation three. The table below shows the improvement of the two parameters:

	ω	β
Baseline	0.0981	58.1485
Point 1	0.0944	57.9676
Point 2	0.0942	57.9830

The table shows (where $\omega=\frac{ptot_{in}-ptot_{out}}{ptot_{in}}$) that the optimization gives good results both in terms of loss coefficient and inlet flow angle, particularly the individual one gives the best value of inlet flow angle, while the second gives the best value of loss coefficient.

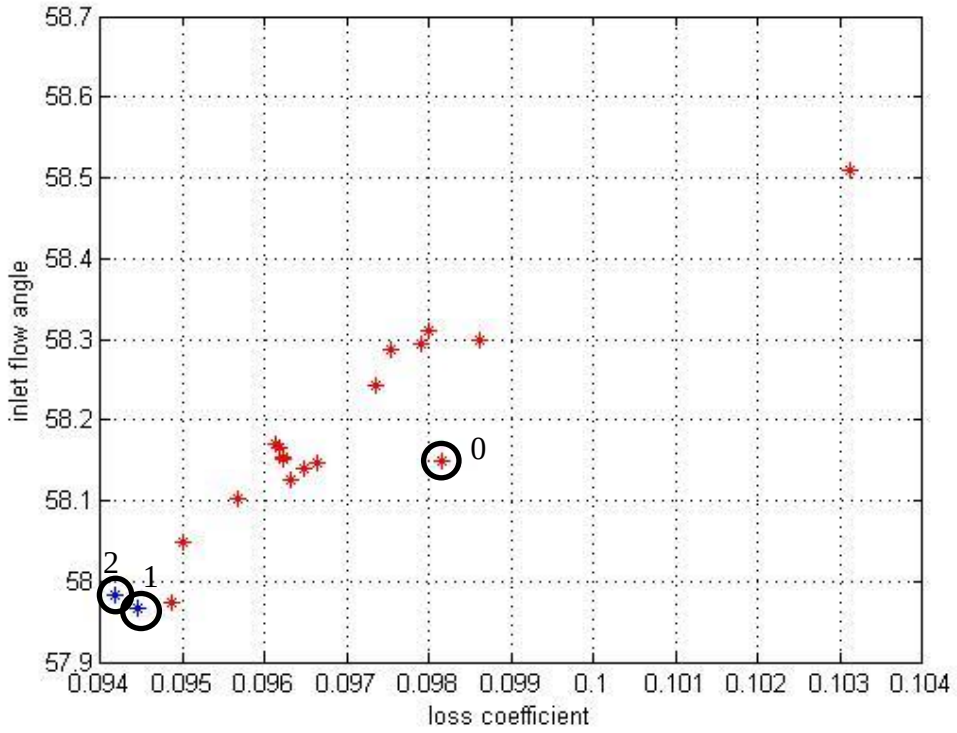

Figure 11.1: Pareto front

Considering the second element, that is the most interesting because of its great improvement in loss coefficient, it is possible to see a decrease in loss coefficient of 4.2% and a decrease in inlet flow angle of 0.29%:

$$\frac{\omega_{baseline}}{\omega_2} = 1.042$$

$$\frac{\beta_{baseline}}{\beta_2} = 1.0029$$

This values express that, even if the inlet flow angle improvement is restricted, the loss coefficient decreases substantially, in fact for a transonic blade an improvement of 4.2% in losses represents a sensible result in performance. Figure (11.2) shows the profile difference between the baseline case (red) and the optimized shape (blue): the optimized shape manifests a longer concave curvature than the baseline, and a maximum thickness downstream on the blade than the baseline. This particular shape is the reason of the differences in Mach number contours that are shown in Figure(11.3) and Figure(11.4).

Observing the Mach number contours appears that in the optimized case from the first zone of the blade departs a greater expansion wave that interests the very first zone of the blade, then the long concave zone, generates a series of compression waves, stronger than baseline one. This compression waves permit the fluid to be more decelerated and so the strength of the shock is reduced. In fact in Figure(11.4) the Mach line of the shock appears not so strong than that in baseline. Moreover also the lambda shock is reduced and the boundary-layer separation shows a reduction in thickness. Hence a reduction in flow velocity before the shock produces a weaker wave with great advantages in terms of efficiency.

In conclusion this simple optimization process certainly is not sufficient to find the complete Pareto front and certainly greater improvement can be find with more individuals and generation, but shows what has been supposed in chapter 8. In fact realizing an optimization process only on the former part of the leading edge permits to decrease the loss coefficient of 4.2% than the baseline case, showing that this part is certainly the most important in the transonic blades, because changes this part involves changes in strength and pattern of shock wave and this is strictly connected with the efficiency of the blade.

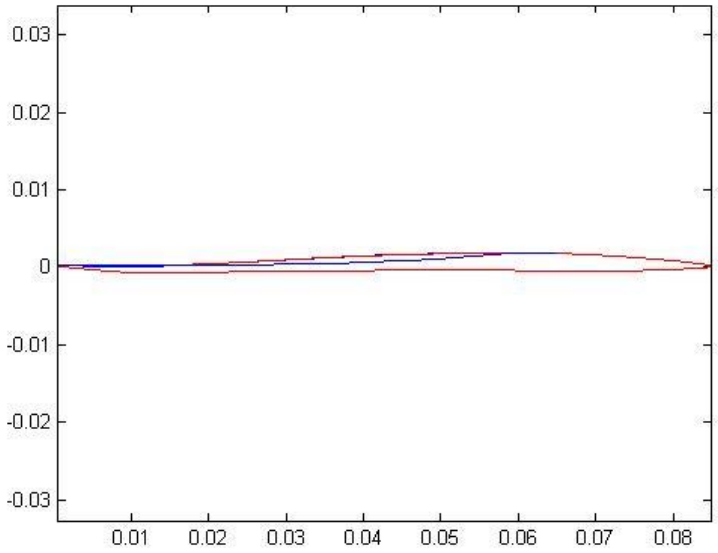

Figure 11.2: Comparison between baseline (red) and optimized shape (blue)

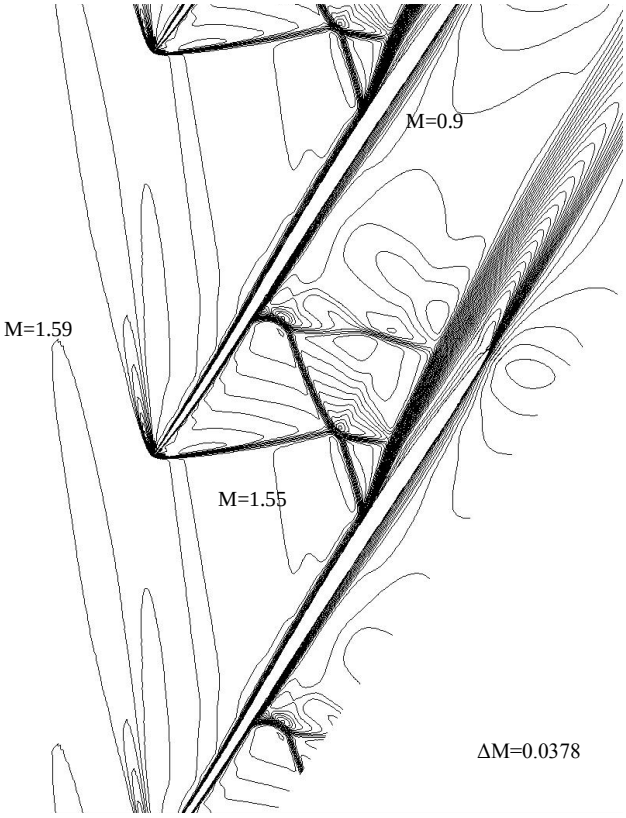

Figure 11.3: Baseline Mach number contours

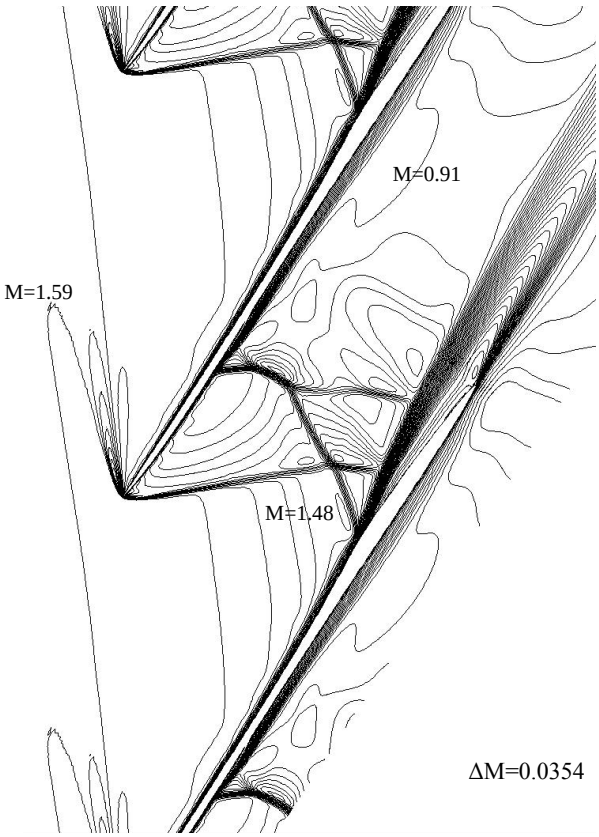

Figure 11.4: Mach number contours of optimized case

12. Conclusions

At the end of this work is possible to fix some guide lines. First the aim of this work is to find the physical phenomena on basis of axial transonic compressor blades and particularly on basis of shock waves that develop in blade passage. The phenomenon of shock wave is the main way whereby the blade compresses the flow, but this phenomenon is strongly complex and of very difficult study. So to analyze the phenomena that happens in transonic blade has been simulated various typology of blades, starting from Kantrowitz blade which is the very first transonic blade, passing through the Double Circular Arc, the Multiple Circular Arc and finally the s-shape profile which is the modern state of art of transonic compressor blades. The blades simulated don't have a three-dimensional advancement but are part of a cascade, so have only a two-dimensional development. This typology of study is important to analyze the shock phenomenon and all the two-dimensional sources of losses. For all these blades has been realized a CAD model from the papers where were reported the dimensions or the coordinates of the blades. Then for each blade has been realized a structure mesh with ANSYS® ICEM, each mesh respects the conditions reported in 4.2 necessaries to have a good mesh. Hence each mesh has been simulated with the computational solver ANSYS® Fluent v14 in order to analyze the fluid domain that is realized by the interaction between the fluid and the blade. The results for each blade have been compared with the experimental results reported in the papers from which have been taken the coordinates of the profiles and so the numerical results have been validated. Now from the knowledge of the fluid domain the physical phenomena that happens in fluid domain is analyzed comparing the different results for the different blades. Comparing the results of the simulations appears clearly that the most important zone of the blade in the compression process is the former zone of the leading edge, where the system of shock waves takes place. In fact the different shapes of this region affect pattern and mainly the strength of the shock wave and this is strictly connected with the efficiency of the blade. From the analysis appears that concave curvature(typical of s-shape) is to prefer because this shape involves a series of pre-compression waves that help the compression process with an oblique shock passage instead a normal shock passage with great advantages in terms of efficiency. After this observations has been decided to realize an optimization process realizing a Bèzier curve parametrization of only the former zone of the suction side that, as already said, is the most important for blade performance and maintaining fix the rest of the blade. So the last part of the work consists in a optimization of the profile in order to evaluate the magnitude of performance improvement (minimize loss coefficient and inlet flow angle) changing this specific zone during the optimization process. The blades has been simulated to find unique incidence

conditions and has been compared in these conditions. The optimization has been conducted with genetic algorithm using 7 individuals and 3 generations, even if both the number of individuals and of generations are not sufficient to find a complete Pareto front the result obtained are however very interesting. In fact the optimization shows an improvement in loss coefficient of 4.2% and of 0.29% in inlet flow angle. This information highlights the changes in performance modifying this part and confirms the idea that this is the more important zone for the blade, because of its influence in shock wave and so in blade efficiency.

A suggestion for future works could be to increase the number of individuals and generations in the genetic algorithm to realize a quantitative optimization and not only qualitative as presented herein. Moreover another possible work could consider the parametrization of all the profile and not only of the first part of the leading edge considering however the importance of the former part. Again it could be interesting to realize the simulations till the spill point conditions that is the most efficiency operating condition.

Ringraziamenti

Al termine di questo ciclo di studi universitario e in particolare di questo periodo di tesi, vorrei ringraziare tuti coloro che con la loro presenza e il loro sostegno hanno permesso il raggiungimento di questo importante traguardo.
Prima di tutto vorrei ringraziare il prof.Benini per la disponibilità che ha sempre mostrato nei miei confronti e, soprattutto, per l'opportunità che mi ha concesso lavorando su un argomento così interessante e stimolante.
Ringrazio Giovanni per tutto ciò che mi ha insegnato in questi mesi e le molte dritte che mi ha suggerito.
Ringrazio la mia famiglia per a fiducia e la serenità che mi ha sempre trasmesso in questi anni di studi, senza che mai nulla mi mancasse.
Ringrazio in particolare Veronica per tutte le volte che mi ha ascoltato cercando di comprendere e risolvere assieme a me assurdi problemi ingegneristici, per tutte le volte che mi ha consigliato, supportato e sopportato; in ansia, anche più di me, ha aspettato questo giorno e mi ha fatto capire quanto sia importante avere una persona cosi al proprio fianco.
Ringrazio tuti gli amici del "college" perché in questo periodo universitario mi hanno fatto comprendere il senso vero e profondo della parola Amicizia.
Ringrazio infine, ma non ultimi per importanza, tutti i compagni di università con cui ho trascorso innumerevoli giornate di studio, il cui aiuto e sostegno hanno reso questi anni, e i molti esami sostenuti, sicuramente più leggeri e meno difficili da affrontare.

Bibliography

[1] Kantrowitz A., Donaldson Coleman duP. ”*Preliminary investigation of supersonic diffusers”* NACA ACR L5D20,1945.

[2] Kantrowitz A. “The *supersonic axil-flow compressor”* NACA ACR L6D02, 1946.

[3] Venturelli,G. “*Development of numerical procedures for turbomachinery optimization “*,Ph.D. thesis, Scuola di Dottorato di Ricerca in Ingegneria Industriale, Universita’ degli Studi di Padova, 2015.

[4] H. Lichtfuss and H. Starken, "*Supersonic Cascade Flow*," 1974.

[5] H. Starken, Y. Zhong, and H.A. Schrieber, "*Mass Flow Limitation of Supersonic Blade Rows Due to Leading Edge Blockage*," in ASME Paper, Amsterdam, 1984, pp. 84-GT-233.

[6] A. Bölsc and P. Suter,” *Transsonische Turbomachinen”*. Kerlsruhe: Braun, 1986

[7] D.L. Tweedt, H.A. Schreiber and H.Starken *“Experimental investigation of the performance of a supersonic compressor cascade”* NASA Technical Memorandum 100879,1988.

[8]Mikolajczak A.A., Morris A.L., Johnson B.V. “*Comparison of performance of supersonic blading cascade and in compressor rotors”* Trans. ASME, Journal of Engineering for Power, vol.1,Series A,pp 42-48,1971.

[9] H.A. Starken and H. Lichtfuss, *"Supersonic Cascade Performance"* AGARD LS 3970 1970.

[10] Creagh John W.R., Klapproth John F. *“Utilization of external-compression diffusion principle in design of shock-in-rotor supersonic compressor blading”* NACA RME53F18,1953.

[11] Lawrence J.Jahnsen, Melvin J.Hartman *“Investigation of supersonic-compressor rotors designed with external compression”* NACA RME54G27a,1954.

[12] Oswatitsch Kl., *“Pressure recovery for missiles with reaction propulsion at high supersonic speed”* NACA technical memorandum MO.1140,1944.

[13] Seyler D.R., Smith L.H. *“Single stage experimental evaluation of high Mach number compressor rotor blading part1-design of rotor blading”* NASA CR54581,1967.

[14] D.L. Tweedt, H.A. Schreiber and H.Starken *"Experimental investigation of the performance of a supersonic compressor cascade"* NASA Technical Memorandum 100879,1988.

[15] T. Sonoda, T. Arima, M. Olhofer, and B. Sendhoff, *"A New Concept of a Two-Dimensional Supersonic Relative Inlet Mach Number Compressor Cascade,"* in Proceedings of ASME Turbo Expo 2009: Power for ALnd, Sea and Air, Orlando,Florida,USA, 2009.

[16] Erwin John R., Linwood C. Wright, Kantrowitz A. *"Investigation of an experimental supersonic axil-flow compressor"* NACA RML6J01b,1947.

[17] H.Starken(DFVLR CO), H.A. Schreiber(DFVLR CO) "*V.4 TEST CASE E/CA-4 LOW SUPERSONIC COMPRESSOR CASCADE MCA*"

[18] H.Starken(DFVLR CO), H.A. Schreiber(DFVLR CO) "*V.5 TEST CASE E/CA-5 TRANSONIC COMPRESSOR CASCADE ARL SL 19*"